Anteroventral thalamic nucleus: Lesion effects on

memory and cortico-limbic electrophysiology

A thesis

submitted in fulfilment

of the requirements for the Degree of

Masters of Science in Psychology

at the University of Canterbury

by Fraser Doake

University of Canterbury

2018

Acknowledgements

I would firstly like to thank Professor John Dalrymple-Alford for his ongoing support and assistance with this thesis. Without your input and advice this project would not have been possible.

A huge thank you also to Brook Perry, Sophie Barnett, and Jenny Hamilton for their help, encouragement, and friendship since I first enrolled at the University of Canterbury. I couldn't have asked for a better lab to have my first experience of conducting research in.

Finally, my sincere gratitude to my partner Tessa, parents Dave and Jill, and brothers Hamish and Cameron for their love, concern, regular 'check-ins', and belief in my being able to finish this project. Your unconditional support during this project has been invaluable and I'm lucky to have such a dedicated team behind me.

Table of Contents

Abbreviations

AD	anterodorsal nuclei
AM	anteromedial nuclei
ATN	anterior thalamic nuclei
AV	anteroventral nuclei
B-L	bregma to lambda measurements
CA1-3	cornu ammonis area 1-3
HPC	hippocampus
Hz	hertz
IEG	immediate Early Gene
IP	intraperitonal
LFP	local field potential
MRI	magnetic resource imaging
MTT	mammillothalamic tract
NMDA	N-Methyl-D-Aspartate
PB	phosphate buffer
PFC	prefrontal cortex
PSD	power spectrum density
RAM	radial arm maze
RSP	retrosplenial cortex
SC	subcutaneous
SUB	subiculum
WE	Wernickes encephalopathy
WB	wideband

Damage to the anterior thalamic nuclei (ATN) is associated with severe memory impairment in humans. What is unclear is how this damage affects electrophysiological activity within an extended hippocampal circuit for memory, of which the ATN is a key component. The current study provides a novel comparison of the electrophysiological activity of rats with lesions to the ATN and intact rats using two electrophysiological measures. These measure are peak power generated by each structure of interest, and the amount of signal amplitude covariance shared by structures, known as coherence. Data were recorded from four key neural memory structures (prefrontal cortex, hippocampus, retrosplenial cortex, and subiculum) during a behavioural paradigm in which rats were presented with novel or previously visited (repeat) arms in a radial arm maze. The current study found decreases in peak power within the sham group when entering repeat arms verses novel. There was also significantly reduced power in rats with ATN lesions compared to shams in the right hippocampus when entering novel arms, and in the right hippocampus and subiculum when entering repeat arms. While there were no significant between group differences in coherence, there was a reduction in coherence in shams when entering novel verses repeat arms in all structures analysed. Overall findings suggest that an intact ATN may play a regulatory role in electrophysiological activity across the extended hippocampal memory system.

Anteroventral thalamic nucleus: Lesion effects on memory and cortico-limbic electrophysiology

Normal memory function is supported in the brain by a distributed network of interconnected structures known as the extended hippocampal memory system. This system is comprised of cortical, diencephalic, and brain stem structures including but not limited to the hippocampus (HPC), anterior thalamic nuclei (ATN), prefrontal cortex (PFC), and retrosplenial cortex (RSP). Damage to, or degeneration of, structures within this circuit is associated with memory impairment. Despite early research emphasizing a hippocampalcentric view of memory, it is now believed that the HPC requires the critical input of these other interconnected structures to facilitate memory function (Papez, 1937; Aggleton & Brown, 1999; Dalrymple-Alford et al., 2015; Vann et al., 2015). One key site in the brain's thalamus, the anterior thalamic nuclei (ATN), shares both direct and indirect connections with the HPC (Jankowski et al., 2013), and is thought to mediate interactions between the HPC and the PFC, another crucial memory structure (Curtis & D'esposito, 2003). Damage to the thalamus often occurs as a result of stroke or alcohol abuse, and can produce memory impairments that have a major impact on patients' quality of life due to this region being implicated in episodic memory, as well as additionally playing a role in the pathology of Alzheimer's disease (Carlesimo, 2011; Kopelman, 2014; Aggleton et al., 2016).

The importance of the ATN for normal memory function is particularly highlighted by the alcoholic Korsakoff's syndrome. Harding et al. (2000) compared patients suffering from Wernicke's encephalopathy (WE), a neurological disorder characterised by thiamine deficiency and neurological impairment, to patients with Korsakoff's syndrome, who show thiamine deficiency and neurological impairment, but critically also have anterograde amnesia. They established that only Korsakoff patients presented with marked atrophy in the ATN, suggesting that this additional damage compared to WE patients was a significant

factor for the anterograde amnesia present in Korsakoff patients (Harding et al., 2000).

Further clinical evidence of the role of the ATN in memory was suggested by an MRI of a

patient suffering from anterograde amnesia and severe loss of verbal memory (Clarke et al.,

1994). The MRI showed the patient had brain damage in the form of dead tissue due to lack

of oxygenated blood supply (known as an infarct), that was largely confined to the ATN and

mammillothalamic tract (MTT; a unidirectional fibre tract from the mammillary bodies to the

ATN). While Korsakoff's and stroke patients produce valuable evidence of the role of the

ATN, the MTT provides a major brainstem input from the mammillary bodies to the ATN,

thus on to the rest of the system due to ATN's numerous connections. If the ATN is

dysfunctional, it deprives the extended hippocampal system of this brainstem input, causing

retrograde degeneration of the mammillary bodies. This is significant because patients with

MTT damage are deemed to have profound amnesia (Carlesimo et al., 2011), and it may be

that the lack of communication from the mammillary bodies to the rest of the system via the

ATN plays a vital role in this memory impairment. This provides further evidence of the

integral role of the ATN and its afferent connections in memory, as well as adding to the pre-

existing literature suggesting a role for the ATN in amnestic disorders.

Clinical studies provide valuable information regarding the various levels and

symptoms of impairments in humans after brain damage, however damage observed in

human brains after stroke or traumatic brain injury is often too widespread to allow

researchers to identify which individual structures or pathways are responsible. To explore

the roles of specific structures in the brain, it is necessary to use animal models to selectively

target regions or structures of interest in order to understand more about their role in wider

memory processes. Early research using rodent models highlighted the role of the ATN in

spatial memory, with ATN damage producing more severe spatial memory deficits on

behavioural tasks compared to lesions to the mammillary bodies, fornix, or even the HPC

itself (Aggleton and Brown, 1999). Further insight into the role of the ATN within the extended hippocampal memory system is provided by Dumont et al., (2010) using a disconnection lesion study. A disconnection study entails subjects receiving single hemisphere lesions to two different structures on opposing sides of the brain (e.g. structure X lesioned in the left hemisphere but intact in the right, structure Y lesioned in the right hemisphere and intact on the left). If these two structures function independently of each other then the intact components should compensate for the lesion in the opposing hemisphere and retain normal brain function, however if they are interdependent then the impaired communication within-hemispheres will result in memory impairment. Dumont et al. (2010) found that a pairing of same-hemisphere (ipsilateral) lesions to the ATN and RSP coupled with a HPC lesion in the opposite (contralateral) hemisphere produced more severe memory deficits compared to any other variation of lesions to these structures. This research further supports the theory of an extended hippocampal memory system, as well as highlighting the crucial role of the ATN and its connections to major memory structures in the brain.

The interconnected nature of this circuit is further emphasised by lesion-induced effects appearing throughout the system, rather than purely within or adjacent to the lesioned structure. Specifically, damaged structures are associated with more widespread neurobiological impacts than would be expected if structures within the system were not working in tandem and instead functioning independently. This means if a structure within the extended hippocampal memory system is damaged, other sites within the circuit show reductions in markers of activity. These 'downstream' effects include altered expression of indicators of neural activity such as immediate early genes (IEGs) and metabolic markers, giving an example of dysfunction within the wider network and providing evidence for the diffuse and interconnected nature of the system (Aggleton & Nelson, 2015; Dillingham et al.,

2015). IEGs are genes implicated in initial cellular and genetic response to stimuli (Tischmeyer & Grimm, 1999) and levels of activation of this category of gene have been examined in distal structures after selective lesions to the ATN. Lesions to the ATN resulted in a global hypoactivation of the IEG *c-fos* in the RSP, as well as often reducing expression in the PFC and HPC (Jenkins et al, 2002; Vann and Albasser, 2009). A second IEG, zif268, which plays an integral role in long term potentiation and spatial memory in the HPC (Jones et al., 2001; Penke et al., 2014) is also reduced in the RSP after ATN lesions (Poirier & Aggleton, 2009; Dumont et al., 2015; Perry et al., 2018). Further examples of distal lesion effects within this system include a reduction of dendritic spine density in the HPC and RSP after ATN lesions, altering the functional status of affected neurons and contributing to observed memory deficits (Harland et al.,2014). A reduction in metabolic function is also observed in the RSP following both ATN and MTT lesions, indicated by decreased levels of cytochrome oxidase (Dupire et al., 2013, Frizzarti et al., 2016). Together, these studies further show how damage to one region within the network can lead to observable effects in other connected structures. This impact on distal structures could be an essential part of the memory deficits associated with brain damage, as while these sites may seem histologically normal they may in fact be functionally lesioned. These studies provide evidence that damage to specific structures within the hippocampal memory system can have an impact on the wider system as a whole, possibly exacerbating the impairment present after ATN damage.

However, examining dysfunction in sites distal to physical damage has its limitations. Many current neural markers, such as the aforementioned IEGs, rely on the use of post-mortem tissue and thus can only be used to establish changes in neurobiology in specific structures rather than across a system, and can show no dynamic or 'real-time' changes, as brain activity is terminated before histology. The current study circumvents these limitations by measuring the electrophysiological activity in the brain through the implantation of

microwire electrodes in key structures of interest within the memory system, namely the HPC, PFC, RSP, and subiculum (SUB). When membranes within the brain are excited, the cumulative local field potentials produced generates rhythmic oscillatory activity in waves that vary in frequency and amplitude (Buszaki et al., 2012). This oscillatory activity is separated into frequency bands, which for the purposes of the current study are defined as delta (1-4 hz), theta (split into low theta 4-8Hz and high theta 8-12Hz), beta (12-30hz), low gamma (30-48hz) and high gamma (52-100hz). Of these bands, theta appears to be particularly involved in normal memory function. McNaughton et al. (2006) showed the fundamental nature of theta for memory processes by using tetracine to inactivate the medial septum, thus abolishing hippocampal theta. Rats lacking in theta activity showed severe impairment in the water maze, however this deficit was ameliorated when hippocampal theta was restored through a bypass circuit, and performance in the maze was returned toward baseline levels. When rhythmic oscillatory activity becomes synchronized across neural structures (known as coherence) it may signal functional interdependence between them. Evidence shows coherence between structures may increase during more complex tasks, suggesting that it can facilitate brain performance in some manner (Fell & Axmacher, 2011; Colgin, 2011). Studies have shown that coherence between the HPC and PFC is integral to spatial working memory in rodents. Colgin (2011, 2013) illustrated that theta rhythms from the HPC entrain PFC firing during spatial working memory tasks, highlighting the necessity of coherence in task performance, as well as the importance of both these neural structures in memory. Jones and Wilson, (2005) show that theta coupling between the HPC and PFC may increase during periods of high cognitive load, specifically during decision making within spatial working memory tasks. The current literature is scarce on studies regarding lesion effects on electrophysiology within the extended hippocampal memory system. The only direct evidence comes from a PhD thesis out of our lab, Perry (2017), who illustrated that

11

lesions to the MTT can decrease theta coherence between the HPC and PFC, highlighting that lesions to structures within the extended hippocampal system may lead to electrophysiological changes between other key memory structures in the system. The current study looks to build on this research by using a modified radial arm maze (RAM) task sensitive to ATN damage to place rats under high cognitive load while recording electrophysiology during a decision making epoch. If rats with ATN damage show diminished theta coherence, it may be that performance and learning during the modified RAM task is impaired, in line with Kim et al., (2011) who conversely demonstrated a progressive increase in theta coherence between the HPC and PFC as rats learnt an object-place pairing, suggesting that theta coherence facilitates learning.

Based on the aforementioned prior research the current study plans to explore any electrophysiological differences between rats with lesions to the ATN compared to sham surgery controls. This will be done by firstly lesioning the ATN, a key memory structure within this circuit due to its dense connections to other structures in the system, and after suitable recovery time then implanting electrodes into structures of interest, namely the PFC, HPC, RSP, and SUB, to record the rhythmic oscillatory activity during an episodic memory task designed to activate the neural circuit. All structures of interest within the current study are implicated in working memory in rats, and share connections (directly or indirectly) to the ATN, thus should show effects after lesion surgery. There are a plethora of studies highlighting the role of the HPC for normal memory function, hence the current study implanted electrodes bilaterally in the HPC, as opposed to all other structures of interest which only received unilateral electrodes. The PFC is a structure of interest in the current study due to its dense connections with other structures within the circuit including the HPC and ATN. The PFC is also crucial for spatial working memory tasks, thus should contribute to performance in a so-called 'forced choice' modified RAM task used by the current study,

in which a mixture of novel and repeat arms are presented one by one to rats placed in the centre hub of a standard RAM (Curtis & D'esposito, 2003; Spellman et al,. 2015). The RSP is also a critical site within the extended hippocampal memory circuit. The RSP is the first structure in the brain to show pathological evidence of Alzheimer's disease in humans, and has been implicated as a site of particular importance with respect to changes at sites within the circuit distal to a damaged structure. As previously mentioned, the RSP shows reduced IEG and cytochrome oxidase activation after damage to distal structures including the ATN and MTT (Harland et al., 2014, Perry et al., 2018, Frizzati et al., 2016), thus the pathways and communication between the ATN and RSP may be crucial for communication and coherence throughout the memory circuit. The SUB is a major output of the HPC, with reciprocal connections to the ATN that are not shared by other components of the HPC (Aggleton & Christiansen, 2015), ergo with successful ATN lesions may show a change in neural activity.

The ATN is a crucial node of communication between the structures of interest in the current study and an integral part of the extended hippocampal memory system. The current study will target the ATN using neurotoxic lesions in order to examine lesion-induced impacts on rhythmic oscillatory activity generated by the structures of interest. We will compare the strength of electrophysiological signals generated at each site across frequency bands (known as power spectrum density; PSD) between lesioned and sham animals, as well as investigating the levels of coherence between the structures of interest. This will be done by recording electrophysiological activity during a modified RAM task, in which the rat is selectively presented with a novel (unvisited) arm or repeat (previously visited) arm. This allows us to explore the rhythmic oscillatory activity as it directly pertains to behaviour, specifically when making decisions within a spatial working memory task. Given the structures of interest are all interconnected within the extended hippocampal memory circuit, and all play vital roles to facilitate normal memory, we expect that there will be disrupted

electrophysiological activity in lesioned animals which will be highlighted when placed under high cognitive load in a behavioural task expected to be sensitive to ATN lesions. Specifically, because of the integral nature of theta in memory we expect diminished coherence between our structures of interest in lesioned animals at this frequency, and a weaker strength of signal (PSD) generated at this frequency by our structures of interest.

<center>Method</center>

Animals

Subjects were 16 male PVGc hooded rats bred in our facility and maintained in standard housing of three or four rats per opaque plastic cage with sawdust bedding (50 cm long x 30 cm wide x 23 cm). The rats were 15-17 months old at the time of lesion surgery and weighed between 320g and 430g. Rats were randomly assigned to either ATN, or sham lesion surgery (control group). Prior to surgery rats were familiarized for 1 week in the RAM. Behavioural testing was conducted during the lights off period (9am to 9pm). Post-operatively rats were individually housed to for 7 - 12 days during recovery. Food and water were available ad libitum during the surgery and recovery period. Pre-surgery familiarization to the RAM, and later behavioural tasks required food restriction to attain 85% of their free feeding body weight, with water available ad libitum. All procedures complied with the University of Canterbury animal ethics guidelines and were subject to AEC approval.

Habituation

One month prior to habituation rats were put on food restriction and their body weight gradually reduced to increase motivation to run for reward. During this period rats were also handled and habituated to the chocolate drops (0.1g) that acted as rewards for the behavioural tasks in the current study. RAM familiarisation prior to lesion surgery lasted for seven days and entailed placing the rats into the RAM in cage groups, with a few (~12) chocolate drops scattered in the central hub, but more liberally down the arms and especially in the food wells at the end of each arm. Each cage group was allowed to explore the RAM for 10 minutes per day for three days and then individual rats were placed for 3 minutes in the maze for the next four days, with chocolate pellets being moved further down the arms towards the food wells each successive day, and doors being raised up and down at random intervals. On the final

(seventh) day of familiarization chocolate drops were placed in only food wells, and doors were lifted and lowered for each arm visit.

Lesion Surgery

An hour prior to surgery rats were given a subcutaneous (sc) injection of carprofen for analgesia (5mg/kg). Rats were anaesthetised with an intraperitoneal (ip) injection of ketamine (40mg/kg) and then a mixture of ketamine (40mg/kg) and domitor (0.35mg/kg) and placed back into a cage until plantar reflex was lost. Following this, 1ml of Hartmanns solution was administered ip to keep rats hydrated throughout surgery. Prior to being placed in a stereotaxic device with atraumatic ear bars (Kopf, Tujunga, CA), rats had the scalp area shaved, which was then cleaned with water and then again using sterile gauze soaked in 4% chlorhexidine gluconate. All items used in surgery were either sterilized prior to use via autoclave, or disinfected through wiping with a combnination of medi-wipes and 4% chlorhexidine gluconate. After being secured in the stereotaxic, the rat was insulated in bubblewrap for warmth and methopt eye drops were administered to keep eyes moist before a tap-water dampened piece of sterile gauze was placed over the eyes to prevent dessication. The incision was made using a sterile scalpel, and a 'splash' mepivicane dose was administered immediately (and intermittently throughout the surgery) for local analgesia. The edges of the incision were secured with haemostats and the sub dermal layers removed to expose the surface of the cranium exposed for the drilling of the infusion holes (Dremel dental drill, Bunnings).

For ATN lesion surgeries the incisor bar was set at -7.5mm below the interaural line in order to minimise fornix damage. In each hemisphere, two infusions were directed at the upper and lower aspects of the anteroventral nucleus (AV), and a third, more anterior infusion was directed at the anteromedial nucleus (AM). One of four AP coordinates was used for

infusions that varied according to the B-L distance (Table 1). Ventrality for AV infusions was -.565 and then -.575 from dura, at ± .152 lateral to the midline, while infusions to the AM were made -.585 from dura and ± .120 lateral to the midline. Neurotoxic lesions were made by infusing 0.15ul of 0.15M NMDA in each site (Sigma, Castle Hill, NSW) in 0.1M phosphate buffer (pH 7.20) at a rate 0.04ul per minute via a 1µL Hamilton syringe (Reno, NV, USA) administered by a microinfusion pump (Stoelting, Wooddale, IL). The needle was left in situ post-infusion for 5 min per site for local diffusion, before being slowly moved to the next site or removed. Sham ATN surgeries used an identical procedure except that the needle was lowered to 1.5mm above the lesion sites and no material was infused. Following infusions, sutures were placed along the incision and emla cleam was applied to the wound. To wake the rat up from anaesthesia a sc dose of antisedan (0.35mg/kg) was administered, along with another 1ml of Hartmans solution. The rat was then held until movement occurred sufficient to establish that the rat was no longer unconscious, and it was then placed in a clean cage with an absorbant pad lining the bottom.

Table 1: Coordinates for infusion sites for ATN lesions

B-L difference	<0.64	0.65-0.68	0.69-0.72	>0.73
AV site to AP (to B)	-.250	-.255	-.260	-.265
AM site to AP (to B)	-.240	-.245	-.250	-.255

Electrode Fabrication

Stepped linear electrodes were fabricated from 50um platinum iridium wire (90% platinum, 10% iridium) with a heavy polyaminde coating (California Fine Wire, CA USA). For each recording site, wires were first cut in to 8cm lengths and then folded in half with the two free ends drawn together. The two ends of the wire loop were then secured with electrical tape. This tape was secured in a pair of straight haemostats and the loop was placed over the arm of

a clamp stand so that the haemostats hung freely below. The haemostats were then rotated ~30 times in a clockwise direction and then 10 times anticlockwise twisting the two taped ends of wire together but keeping a distinct loop above the conjoined ends. Gentle heat was then applied from three directions, fusing the polyamide coating of the wire along the twisted end. Additional strength was given to each electrode by applying a thin coat of cyanoacrylate to the twisted section of the wires. Each linear array consisted of two (CA1) or three (PFC, RSP, SUB) unipolar electrodes drawn against each other to different lengths so electrode tips could be placed in different structures/subregions in the dorso-ventral plane (Figure 1). Electrodes in each array were first cut to approximate length using a fresh scalpel blade and then a small amount of nail varnish (a different colour for each electrode) was applied to the loop so the position of each electrode could be identified. Each of the electrodes in each linear array was then threaded through a 3mm piece of 23 gauge stainless steel cannula (PlasticsOne). Each electrode was then manipulated along the array under a dissection microscope to the correct depth and fixed in place with cyanoacrylate.

To aid implantation of each electrode array a gold milmax pin was superglued to the top of the cannula so the line of the pin was parallel to the electrode wire. Once the cyanoacrylate was fully dried (overnight), the apex of the loop on the untwisted end of the electrode was exposed to an open flame to remove ~ 15 mm of the heavy polyamide coating to allow it to be soldered to a milmax connector. The two sides of the loop were then drawn together and the uninsulated section given a liberal coating of flux and then wrapped 2-3 times around one pin of a milmax connector (cut into a square of 2x2 pins) before being soldered in place. Care was taken to ensure no electrode was touching more than 1 pin. Once each electrode in an array had been soldered to a milmax pin, all electrodes were tested to ensure current flowed easily through the pin down to the electrode tip. For this, the tip of the array was placed in a petri dish of saline, connected to the negative lead of a DC power

source, which was secured under a dissection microscope monitored by a live video feed (Nikon, Japan). A 5V current was then passed down each electrode separately. Sufficient flow of current resulted in the formation of bubbles at the tip of each electrode. If bubbling was not apparent or bubbling occurred at all tips in the array, the tips of the electrodes were re-cut and solder connection checked. Any array that could not be fixed was discarded and a replacement electrode fabricated. Following testing, a small amount of epoxy resin was placed over the top of the soldered pins for added strength and insulation. Ground wires were constructed from 12cm lengths of 200um pure silver wire. One end of the wire was soldered to the head of an anchor screw and the other soldered to a four connector bank of milmax pins (AM Systems).
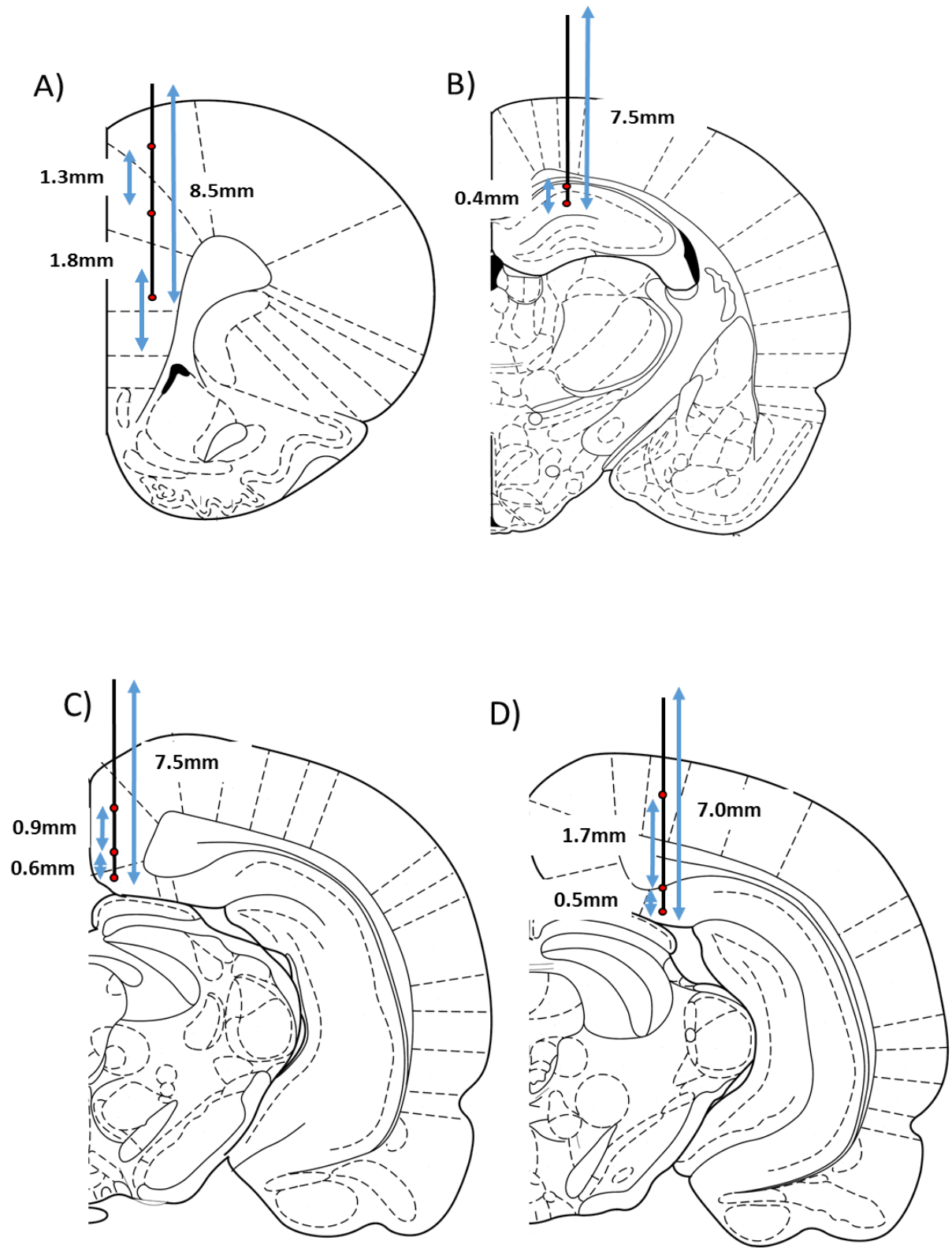
Figure 1: Distance from canula to deepest tip of electrode, and distance between stepped electrode tips for A) Prefrontal B) Hippocampal C) Retrosplenial and D) Subicular electrodes.

Electrode surgery

One hour prior to surgery the rats were given carprofen to provide analgesia (5mg/kg; s.c).General anaesthesia was induced by placing the rat in an induction chamber with a mixture of 4% isoflurane and oxygen at a flow rate of 1000ml/min. Once the righting reflex was no longer apparent and the animal's respiration rate had slowed, it was removed from the induction chamber, administered supplementary fluids (1ml hartmans solution; i.p), and the scalp shaved and wiped clean with a fresh damp paper towel and 4% chlorhexidine gluconate. Before the rat regained consciousness, it was placed back into the induction chamber to maintain anaesthesia, and then secured in the nose cone of the stereotaxic frame. Once in the stereotaxic, the concentration of isoflurane was lowered to a 2% maintenance dose. Waste gases were passively scavenged into the outside atmosphere via an exhaust system and all anaesthesia equipment were cleaned and disinfected with medi-wipes before and after use. If the animal appeared responsive to tail pinch or plantar reflex during regular observations, or showed other signs such as whisker movement, the isoflurane rate was increased to 4% until reflexes were lost, at which point the isoflurane rate was reduced back to 2%. A surgical plane of anaesthesia was then confirmed by the loss of tail pinch and plantar reflexes. Observations were repeated at every ~10 mins during the surgery as well as visual checks of colour and respiration. The rat's body was kept warm during surgery through insulation in bubble wrap. Methopt Forte eye drops were applied before the addition of damp gauze placed above and clear of the eyes, to prevent dessication during surgery. The site of incision was then disinfected with sterilized gauze soaked in 4% chlorhexidine gluconate. Following incision with a sterile scalpel the rat was given local analgesia 'splash' applied directly to the wound (0.2ml of 2mg/ml of Mepivacaine). The sides of the incision were retracted and held in place with curved haemostats and the sub dermal layers removed to expose the surface of the cranium. The surface of the skull was then crossed hatched with a sterile scalpel blade to increase adhesion of the dental acrylic. Eight small holes were then drilled (at a 45 degree angle) around the perimeter of the skull for the

insertion of jewellery screws; six in the left and right parietal bones to provide anchoring points, one in the frontal bone to act as a ground, and one in the occipital bone above the cerebellum as an indifferent reference. Once all the screws were fixed in place, the silver wire attached to the ground screw was wrapped around the six anchoring screws. Next, a dummy electrode was secured in a female milmax plug and using bregma, lambda, and the mid sagittal suture as reference points, small craniotomies were made above the location of the PFC, bilateral HPC, RSP, and SUB array using the coordinates in Table 1. Each array was then inserted one at a time starting with the PFC, then the left CA1, right CA1, dorsal SUB and the RSP. Once each array had been lowered to the correct depth (taken from dura) it was fixed in place with a small amount of dental acrylic. Once all five arrays were fixed in place, additional dental acrylic was used to fill in any gaps between the electrodes to form the base of the head cap. The gold milmax pins used to aid insertion of the arrays were then removed and the six 2x2 milmax connectors (5 arrays plus the ground/reference) were plugged into a dummy plug to hold them in the correct position to interface with the headstage. The headcap was then built up with additional dental acrylic to cover all the wires and fill in any remaining gaps between the electrodes, as well as hold the dummy plug made from the milmax connectors in place. Once the acrylic had set, the dummy plug was removed and the tissue around the headcap cleaned with sterile saline. Following this, the Plexon system was plugged into the headcap and a recording was taken while the rat was still under anaesthesia to ensure all electrodes were transmitting. A suture was added if necessary at the posterior end of the incision. Emla cream was then applied to the wound, the isoflurane vaporizer turned off, and the oxygen flow rate raised to 2000ml/min to promote recovery. The rat was then removed from the stereotaxic and placed in the induction chamber where it received an additional 2 minutes of pure oxygen, and given 1ml of Hartmans solution ip, before being placed in a clean cage to recover. Rats were kept in single housing, in a recovery room for 7 days post-surgery, and checked at least twice a day for any signs of pain or distress. Following this, rats were re-housed in groups of 3-4.

Table 2: Co-ordinates for electrode implantation at our designated site. Laterality coordinates are taken from midline, while depth coordinates are taken from Dura.

B-L distance	≤ 0.64	0.65-0.68	0.69-0.72	≥ 0.73	Laterality	Depth
PFC recording site	+0.210	+0.215	+0.220	+0.225	+0.06	-0.400
HPC recording site	-0.290	-0.295	-0.300	-0.305	+/-0.21	-0.250
RSP recording site	-0.485	-0.490	-0.495	-0.500	+0.07	-0.270
SUB recording site	-0.530	-0.535	-0.540	-0.545	+0.28	-0.340

Electrophysiological recording

Electrophysiological data was recorded with the OmniPlexD Neural data acquisition system (Plexon, Tx). The implanted electrodes were connected to the system via a custom made *Milmax*/Omnetics adapter consisting of a bank of Milmax pins in the same configuration as the rats headcap, then soldered onto a 16 channel electrode interface board (Neuralynx, Mo) which directly connected to the Plexon digital headstage via an Omnetics connector. Single electrode signals were referenced to ground, filtered between 0.05 and 8 kHz (wideband signal; WB), multiplexed and digitized by the headstage and sampled up to 40kHz by the digital head stage processor (DHP). Digital signals were transmitted over a data link cable to an acquisition card connected to a computer running Omniplex server and Plexcontrol software. Local field potentials (LFP) and WB were recorded separately. LFP was sampled at 1 kHz and filtered between 0.05 Hz and 200 Hz. All recorded channels were saved to the computer running the OmniPlexD software for offline analysis in Neuroexplorer version 5, Matlab, Windows Excel and SPSS.

Behavioural testing:

Standard RAM test post-lesion surgery

Following lesion surgery (and recovery period) rats were maintained at 85% of their free feed weight and tested for 15 consecutive days of a standard working memory procedure in the 12-arm RAM, without re-baiting the wells within trial. The 12-arm RAM used in the current study was situated in a windowless room measuring 3.35m by 3.30m, with different objects mounted on each wall as well as a curtain and two desks, to allow the rat to use allocentric cues to orientate itself. The RAM central hub and arms were raised 71cm off the ground, and arms measured 65cm by 9.5cm. Perspex doors that could be used to block off each of the 12 arms were 27cm high by 9.5cm wide, and each arm was attached to a pulley system so it could be raised and lowered individually from other arms. At the start of each trial, the rat was placed in the central hub and after a ~10 second delay all 12 clear Perspex doors were lowered to allow the rat choose an arm (both back legs past the threshold, with no back tracking). On entering an arm, the doors were raised and the rat was allowed to consume the food reward if present and return to the hub. Each trial concluded when the rat had visited all 12 arms, 20 arm choices had been made, or 10 minutes had elapsed.

An identical method RAM was used after electrode surgery (and recovery period) for 10 days, but electrophysiological recordings were now also taken during, in order to assess changes in neural activity throughout the task. Each rat was plugged in to the electrophysiology recording system via a 'male' plug attached to the Plexon system being inserted into the 'female' receptor built into the rat's head cap. The rat was then placed into the centre hub of the maze and the electrophysiology software was initiated, before recording and testing began. To ensure accurate pairing of behaviour and electrophysiological activity infrared beam breaks with a diameter of 3mm, consisting of a transmitter opposite a receiver (Adafruit Industries), were fixed 3cm above the floor of each arm at two locations. The first transmitter/receiver was located 15cm down the arm to

mark arm entry, and the second placed 12cm before the end of the arm (just before food well was reached) giving 38cm between beam breaks within each arm. Beam breaks were powered by two separate 5 volt DC power outputs coming from analogue I/0 ports on the Plexon chassis, each supplying power to six arms. To read a digital signal when the infrared beam was broken, a 10k resistor was soldered between the signal and power wires of the infrared beam receiver. The signal wires from each of the 24 infrared receivers were fed into the digital input card on the Plexon chassis and automatically timestamped on the Plexon file with 25 microsecond resolution when the infrared beam was interrupted by a rat.

Forced choice RAM task

Following the standard RAM procedure animals were then tested for 12 days in a modified procedure using only one open arm at a time for a sequence of 14 arm presentations. Novel arms were presented for the first 8 arms, and then a combination of 3 repeat arms and a further 3 novel arms were presented across the last 6 arms opened to the animal. Repeat arms were counterbalanced across trials and each set of 3 repeat arms within a trial contained an 'early', 'middle' and 'late' repeat arm, referring to when the arm was initially presented as novel within the trial verses when the arm was presented as a repeat. There was a total of six 14-arm sequences which were cycled through across the 12 days of testing. Rats were placed into the centre of the maze with all arms raised for ~10s and electrophysiology recording software was initiated before the first door was lowered. Timestamps were taken from when the Perspex door was lowered and were compared using the time stamp of the 1st beam break down the opened arm to produce a latency measure of animals entering an arm. Once the animal had ventured down the arm, obtained the food reward, and returned to the central hub, all arms were again raised before the next arm was presented. If an animal did not venture down the open arm within ~8s, the door was raised and the testing proceeded

to the next arm in the trial sequence. The trial concluded when the animal had been presented with all 14 arm presentations within a trial. As with the previous RAM task, electrophysiological activity was recorded throughout each trial.

Data analysis

Local Field potentials

Local field potentials (LFP's) from the prefrontal, hippocampal, retrosplenial, and subicular electrode arrays were processed using Neuroexplorer version 5, matlab, and Microsoft excel. For each rat, one suitably positioned patent channel per site was selected after histologyfor all analyses of LFP's. Raw LFP data was first notch filtered at 50Hz with 1Hz notch width to remove line noise and then bandpass filtered between 1 and 110 Hz for recordings taken during surgery (not reported here), and 2.5 and 100 Hz for recordings made during behavioural tasks. The band pass filter employed by Neuroexplorer is similar to matlabs filtfit function. Before spectral and coherence estimates were calculated, the filtered LFP channels were visually inspected for obvious interference from noise and any channels or recording segments showed such artefacts were discarded. The frequency spectrum was broken down into the following frequency bands for all analyses; delta (1-3.9 Hz), low theta (4- 8 Hz), high theta or alpha (8-12 hz), beta (13-30 Hz), low gamma (30-48 Hz) and high gamma (52-100 Hz).

Multitaper spectral estimation

Spectral analyses were performed separately for each patent electrode across the five recording arrays in each rat in using the multitaper spectral estimation function (time bandwith product = 3; number of tapers = 3) with a 90% window overlap in Neuroexplorer This technique takes advantage of short time window Fourier analysis to reduce artefacts
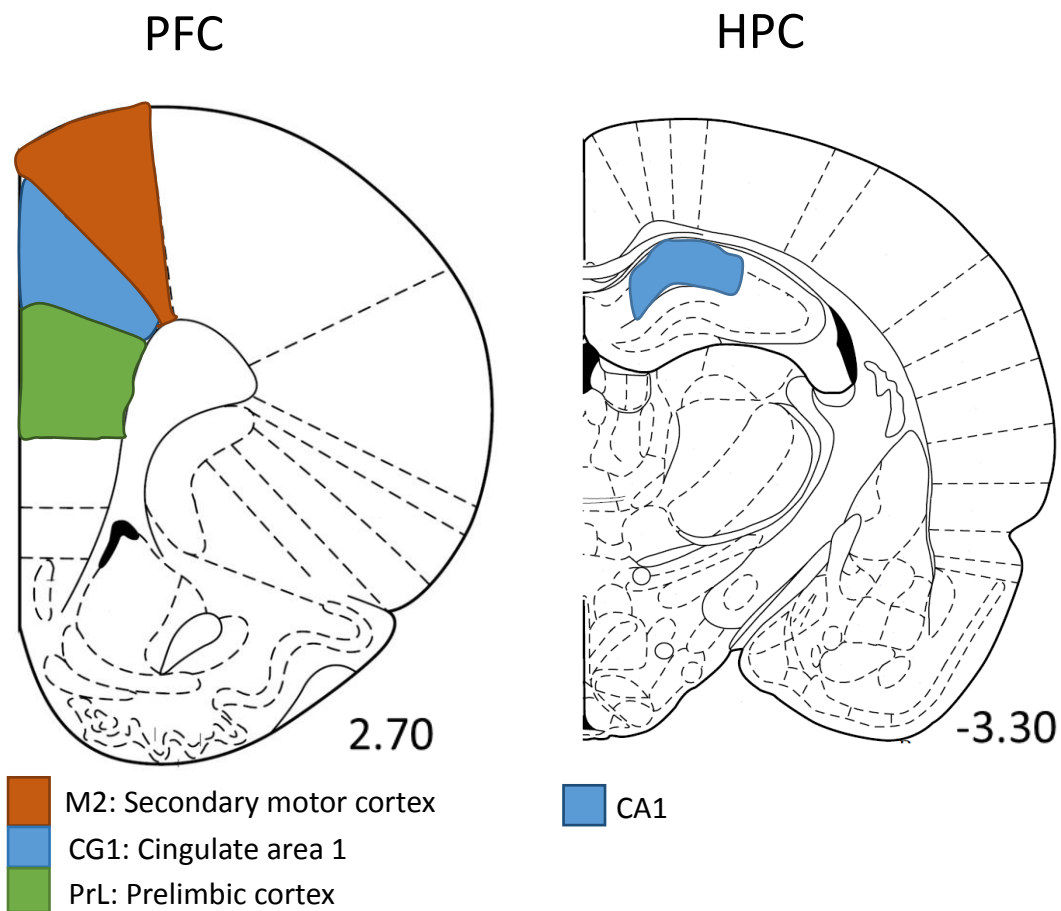
26

caused by non-stationary elements in the data, since data can be assumed to be stationary within the short sliding time windows (Jones & Wilson 2005). For each spectral analysis, each window was pre-processed by subtracting the mean within each window before the tapers were applied. The data were smoothed with a Guassian filter (3 bin filter width) and sent directly to excel or matlab for further processing. To allow for effective comparisons across animals and recording sessions, data were normalised using matlab's zscore function, which creates a new distribution for each power spectrum density (PSD) with a mean of 0 and a standard deviation of 1. This normalisation procedure accounted for variance in signal amplitude across recordings and animals as a result of factors such as electrode impedance and slight variations in location. Peak power was then calculated and compared by taking the maximum normalised power for each region within each band per rat. The assistance of Dr Brook Perry with these analyses is acknowledged.

Coherence analysis

Coherence is a measure of the covariation between two electrophysiological signals conducted within each frequency band. This measure was estimated in Neuroexplorer using the same multitaper parameters described above. Coherence coefficients were calculated between the HPC-PFC, left HPC- right HPC, and HPC-SUB separately, using the 1-100Hz bandwidth during behavioural testing. Data were exported from Neuroexplorer into Microsoft Excel. Only coherence coefficients between ipsilateral electrodes were retained. Again, peak coherence and AUC's in each separate frequency band were calculated and compared across groups.

Regions of interest

For reasons outlined in the Introduction, the current study implanted 5 electrodes across 4 regions of interest: the PFC, the HPC (bilaterally), the RSP, and the SUB. The electrodes used in the current study had stepped tips so it was possible that more than one electrode was located in each of our regions of interest (Figure 2). Data from only the most appropriately located electrode tip was analysed.
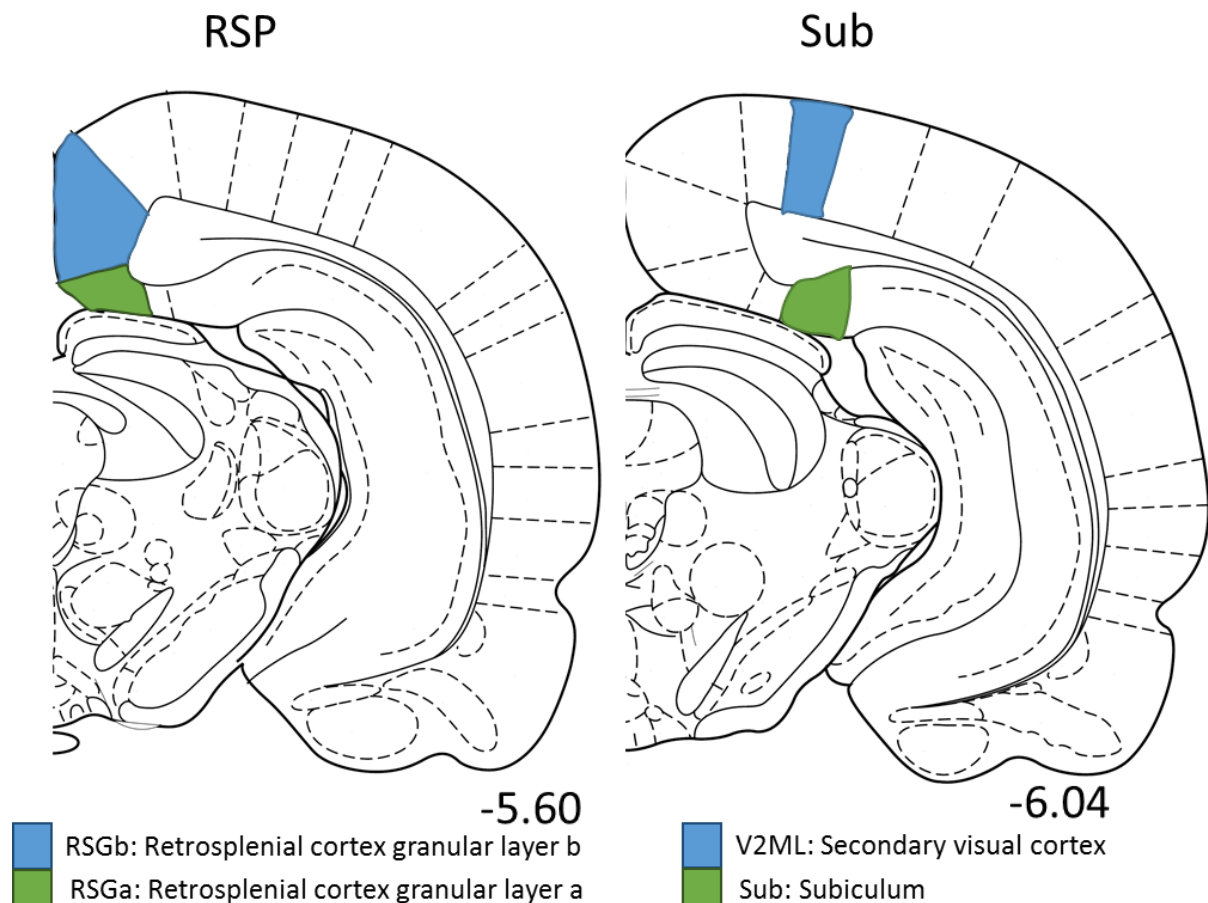

PFC   HPC

2.70   -3.30

■ M2: Secondary motor cortex   ■ CA1
■ CG1: Cingulate area 1
■ PrL: Prelimbic cortex

RSP   Sub

-5.60   -6.04

RSGb: Retrosplenial cortex granular layer b
RSGa: Retrosplenial cortex granular layer a

V2ML: Secondary visual cortex
Sub: Subiculum

Figure 2: Atlas plates depicting regions of interest for intended electrode implants in the current study, with distance from Bregma for each plate.

Histology

After the final day of testing rats were deeply anaesthetised with sodium pentobarbital (125mg/kg) and perfused transcardially with ~200mls of chilled saline followed by ~200mls of 4% paraformaldehyde in a 0.1 M phosphate buffer (PB) solution (pH 7.4). The brain was extracted and post-fixed in 4% paraformaldehyde overnight, before transfer into a long term solution (20% glycerol, 0.1M PB and distilled water; Ph 7.4) for a minimum of 48 hours.

Coronal sections (50μm) from approximately - 0.92 to -3.30 from Bregma (to encompass the ATN) were taken using a sliding microtome with a freezing stage

(Thermoscientific, UK). Tissue sections were stored at -20º C in a cryo-protectant solution (30% glycerol, 30% ethylene glycol and 40% 0.1M PB) until processed for lesion verification. For electrode verification, 50µm coronal sections were taken from Bregma +4.20 to +1.00 for PFC electrodes, Bregma -2.12 to -4.52 for HPC electrodes, Bregma -4.80 to -6.80 for RSP electrodes, and Bregma -6.04 to -7.30 for SUB electrodes. Sections were then stained in cresyl violet for verification.

Cresyl violet staining

Sections were washed for 2×10 mins in 0.1M phosphate buffered saline, and then for 2×10 mins in 0.05M PB to remove the cryo-protectant solution. The sections were then mounted from deionised water on to gelatine coated slides and allowed to air dry overnight before staining. Slides were delipidised in graduated concentrations of ethanol and then rehydrated in distilled water before being incubated in fresh standard cresyl violet solution for 8 minutes (to maintain similar stain density). The slides were then dehydrated and differentiated in graduated ethanol solutions and acid alcohol respectively, before being cleared in xylene baths and cover-slipped with DPX mounting solution.

Lesion and electrode verification

The ATN is comprised of 3 main nuclei: the anterodorsal nuclei (AD); anteroventral nuclei (AV); and anteromedial nuclei (AM); but for the purposes of the current study these are jointly referred to as the ATN. ATN lesion sections stained with cresyl violet (a Nissl stain) were observed with a stereomicroscope (Nikon, Japan) by John Dalrymple-Alford who was blind to the rats' prior behavioural performance. ATN Lesions were accepted when visual inspection indicated ~50% or more bilateral ATN damage, minimal fornix damage, and little obvious evidence of damage (clearly below 50%) to immediately adjacent regions. Any cases with extensive unilateral or bilateral sparing were excluded from further analysis. Electrode

placements were also observed via stereomicroscope. Prior to perfusion of each rat, each electrode was stimulated at 20μamps for 20s per electrode via an open source pulse generator (Pulsepal V1.0; Sanders and Kepecs, 2014), creating a small electrolytic lesion at each electrode tip for verification of electrode placements. Inaccurately placed electrodes were excluded. Included electrode sites were located in the prelimbic region for the PFC, in the CA1 region for the doral HPC, and the subiculum cortex for the SUB.0

Lesion verification

As described above, rats with ATN lesions were included when visual inspection indicated

about 50% or more bilateral ATN damage, minimal fornix damage and little obvious

evidence (below 50%) of damage to immediately adjacent regions (Dalrymple-Alford et al,

2015; Loukavenko et al., 2016; see Figure 3). 3 rats were excluded due to incomplete lesions,

leaving a final sample size of 4 rats with ATN lesions. 1 sham rat was excluded on the basis

of incorrectly placed electrodes, leaving a group of 8 sham surgery controls. An example of a

successful lesion compared to a sham surgery can be found in Figure 4.
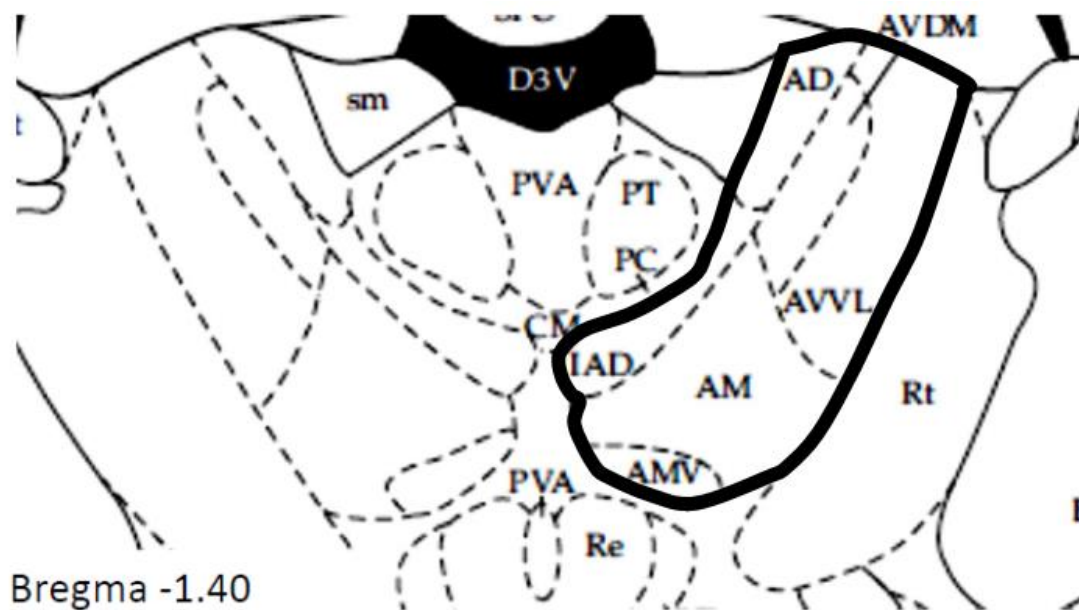
Figure 3: Atlas plate showing the nuclei comprising the ATN (outlined) and its adjacent structures
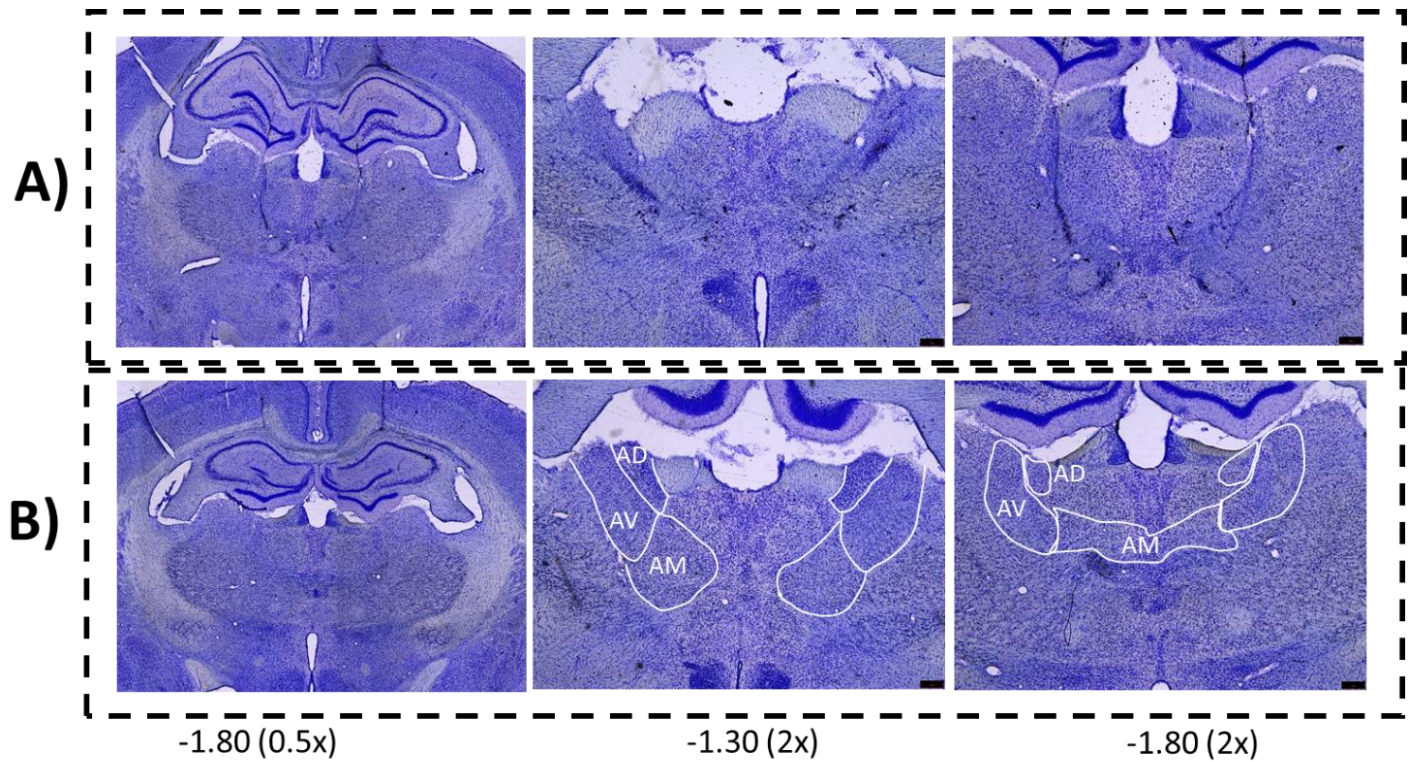
Figure 4: Photomicrograph of a successful ATN lesion (Row A) and sham surgery control (Row B) at two different anterior-posterior coordinates. Constituents of the ATN are labelled in the sham sections. Sections were stained with cresyl violet.

Electrode Verification

Electrode placements were verified by John Dalrymple-Alford using a stereomicroscope. Figure 5 shows where electrode tips in the current study were placed including exclusions for the PFC (2 rats excluded) and SUB electrodes (3 rats excluded). Due to time constraints, RSP electrodes could not be identified accurately enough to be included in analysis.
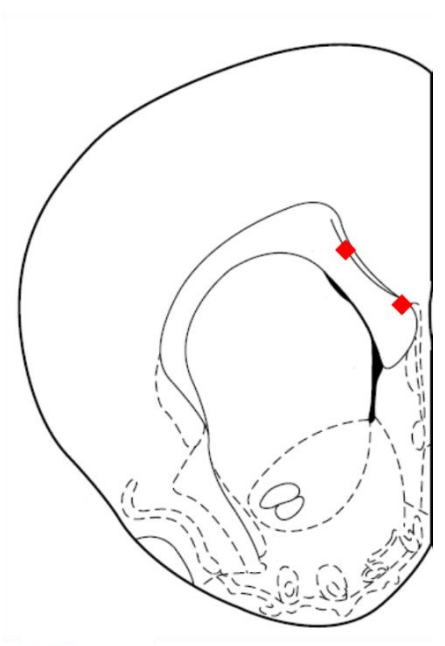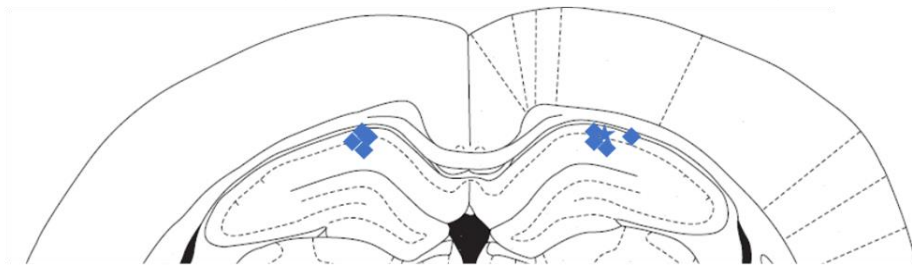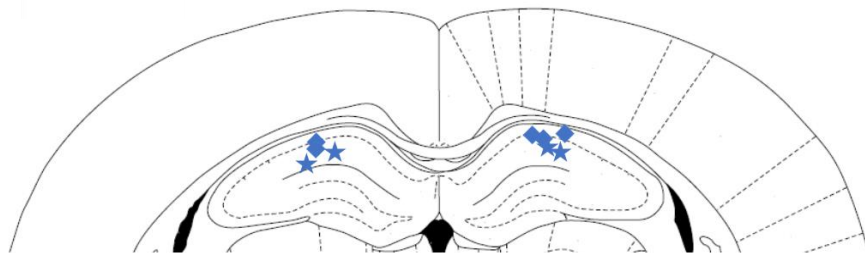
5.1)
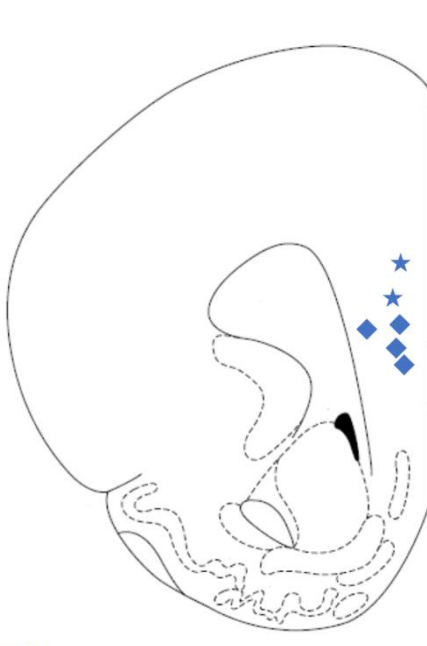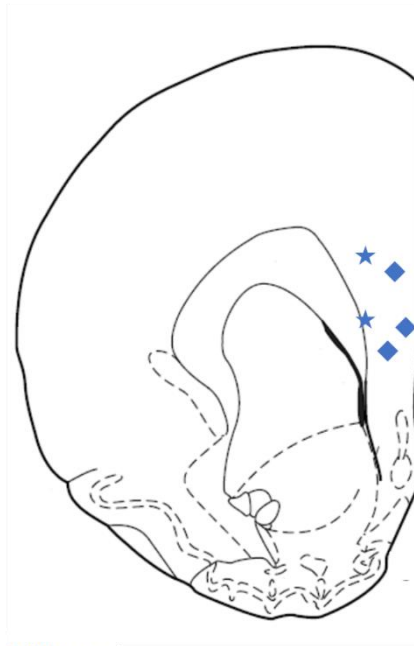
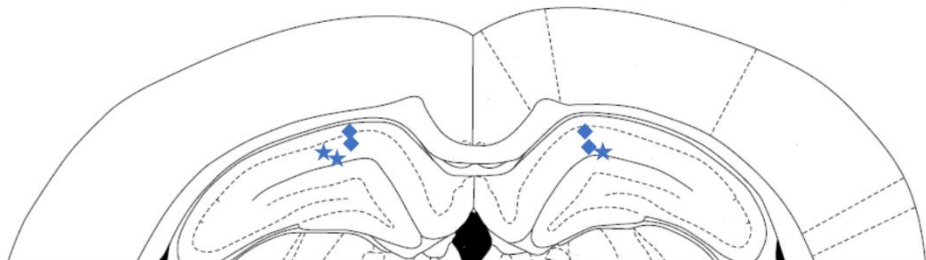2.70 mm   2.20 mm   1.70 mm

5.2)

-3.60 mm

-3.30 mm

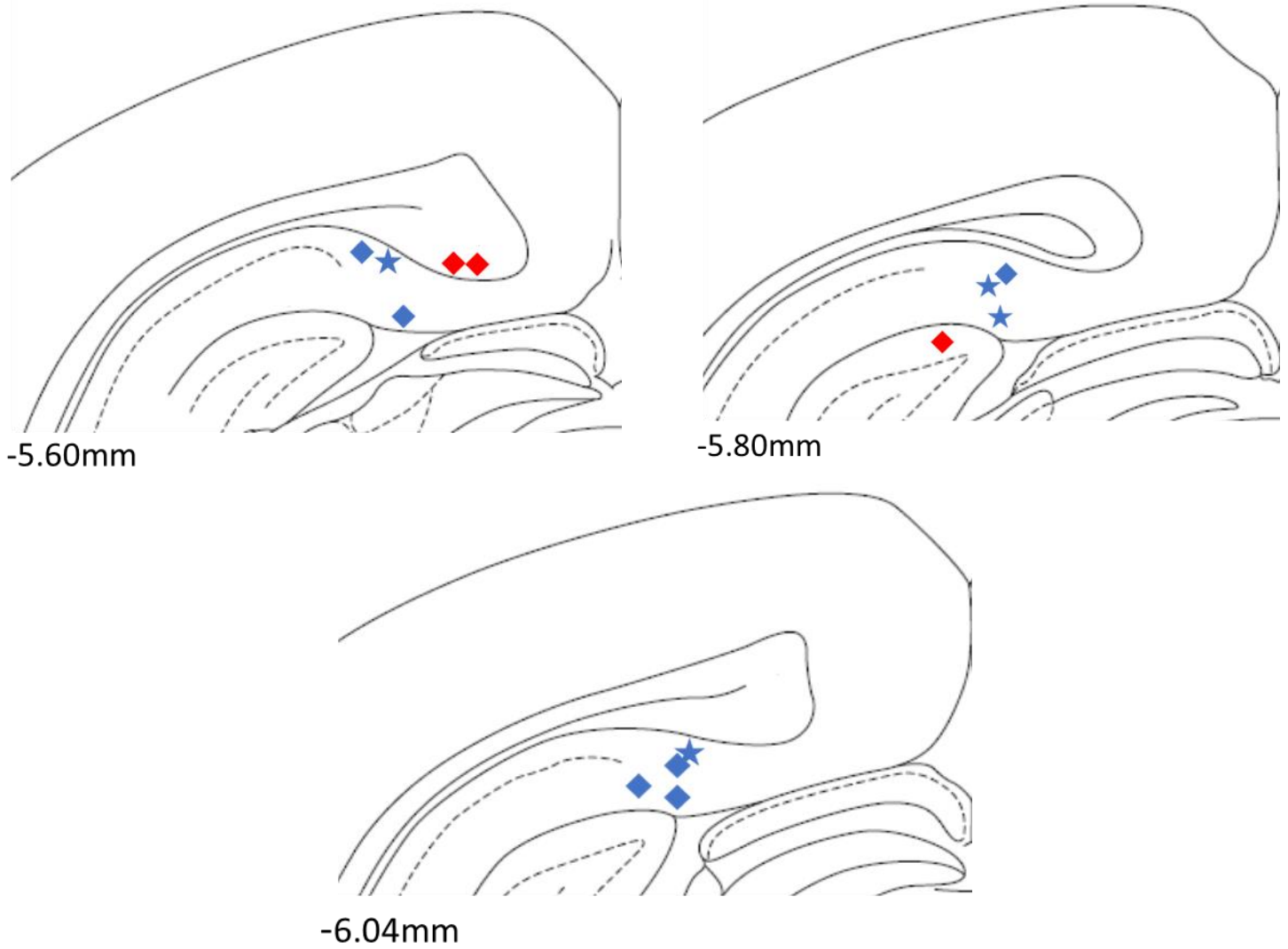-4.16 mm

5.3)

-5.60mm

-5.80mm

-6.04mm

Figure 4.1 Coronal atlas plates indicating the approximate location of all prefrontal cortex electrodes in both the sham and ATN group. Stars denote ATN rats and circles denote sham rats. Red symbols indicate cases excluded from data. Figures 4.2 and 4.3 show hippocampal, and subicular electrode placements, respectively.

.

Spatial working memory in the RAM:

Rats were tested on a standard RAM task after lesion surgery, prior to electrode surgery as a behavioural measure of lesion efficacy. Across 15 days of testing, lesions increased RAM errors relative to the sham group (Lesion main effect: $F_{(1, 12)} = 10.90$, $p<.01$) (Figure 6). There was also an effect of across days ($F_{(1, 14)} = 10.84$, $p<.001$) but not of group by day ($F<1.0$).
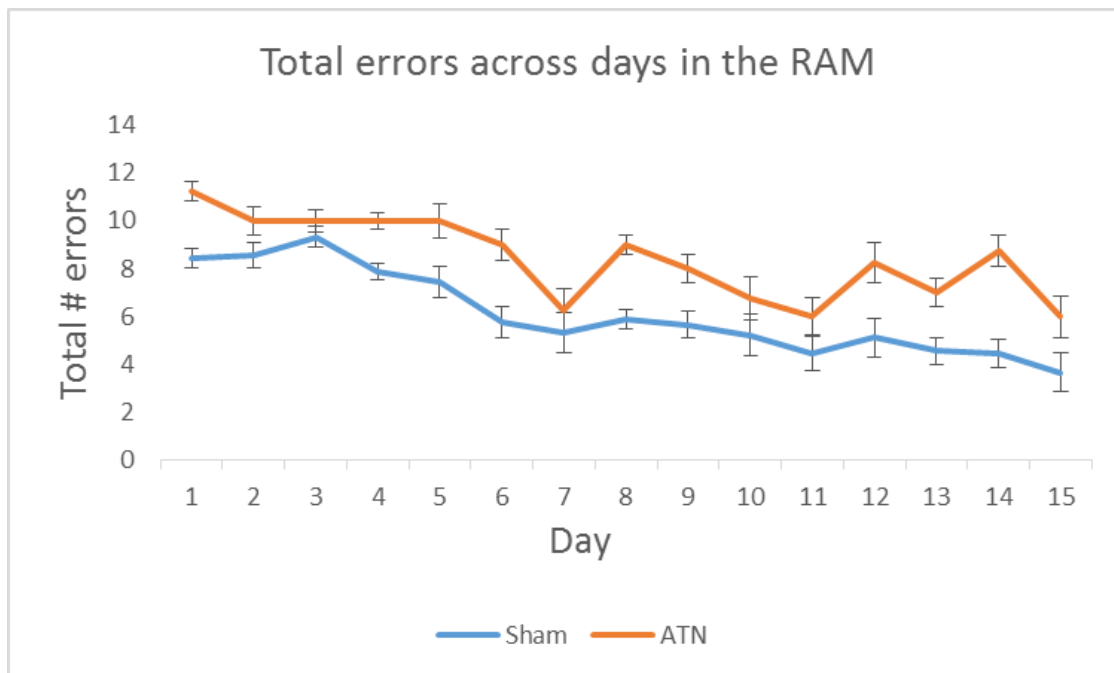

Figure 6: Total number of errors across days in both lesion and sham rats in the standard RAM task after lesion surgery

Electrophysiology

The 0.5s electrophysiological epochs used for analysis were taken from 0.7s-0.2s before the first beam break was broken in any given arm. This provided a 'decision point' of the rat entering an arm. Electrodes placed in the RSP were not included in the current study as time constraints prevented accurate identification of electrodes in this structure. Because of the

large number of statistical tests required to examine each frequency band separately it was not feasible to control the family-wise Type I error using standard parametric statistics. There was also unequal variance and non-normally distributed data between the sham and ATN lesion groups. A Mann-Whitney U test was subsequently used to compare peak values in each frequency band between the sham and ATN lesion groups and a Wilcoxon rank sum test was used to analyse within-subject measures. Importantly, the family-wise Type I error was controlled by using an p value calculated for each test using a Monte Carlo estimation which permuted the data 10000 times and gave a 99% confidence interval (CI) around the p-value (Maris & Oostenveld, 2007; Maris et al., 2007)**.** Analysis on electrophysiology recorded at dorsal hippocampal CA1 (HPC), medial prefrontal cortex (PFC) and subicular cortex (SUB) electrodes is presented.

Power Spectrum Density

Peak power during novel vs repeat arm entry – within-group analyses

Analysis of power spectrum density within each group showed no significant differences in peak power in the lesion group at any frequency band between novel and repeat arms in the PFC, HPC, or SUB (Figure 7). The novel verses repeat arm PSD electrophysiology for sham rats is shown in Figure 8. In the sham group, a significant decrease in high theta in the subiculum was evident when entering repeat arms compared to novel arms (Z = -2.310, Monte Carlo *p* = .02, 99% confidence interval = .016 - .024). In the sham group, there was also a decrease in both delta and low theta approaching significance in the PFC (both Z values = -1.96 Monte Carlo *p* =.054, 99% confidence interval = .048 - .06) which further extended to a decrease in delta frequency in the left HPC (Z = -1.96, Monte Carlo *p* = .055, 99% confidence interval = .049 - .061*)***.**

Normalized PSD in lesioned rats entering novel and repeat arms

Figure 7: Mean normalized power ± SEM for lesioned rats entering novel (green) and repeat (red) arms as generated by the A) PFC, B) left HPC, C) right HPC, D) SUB. Thickness of lines indicate standard deviations in the data. No significant differences were found for peak power within any frequency band. Data were analysed separately for each of the following frequency bands: Delta – 1-4Hz; Low theta – 4-8Hz; High theta 8-12Hz; Beta 13-29Hz; Low gamma 30-48Hz; High gamma – 52-100Hz

Normalized PSD in sham rats entering novel and repeat arms

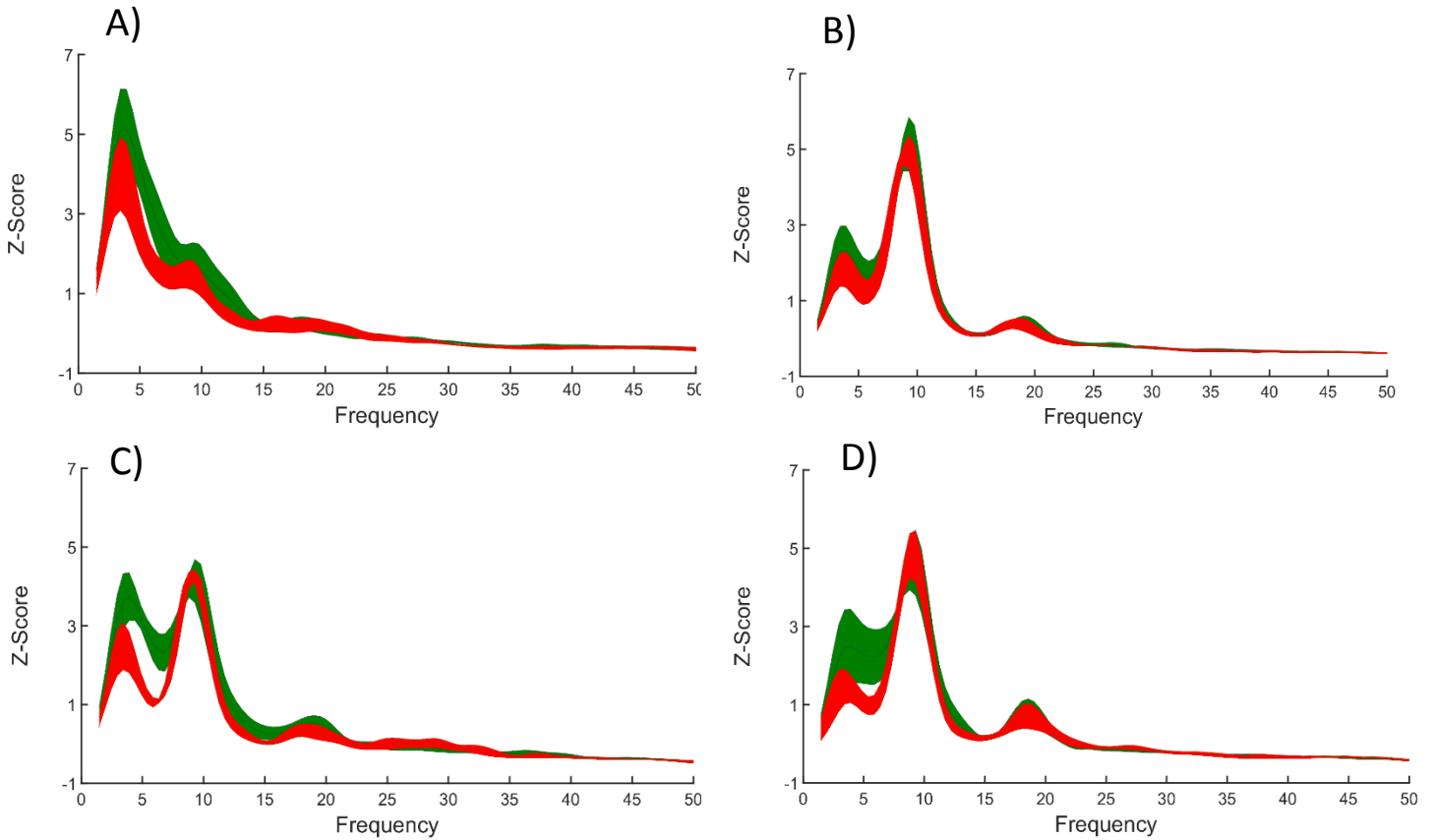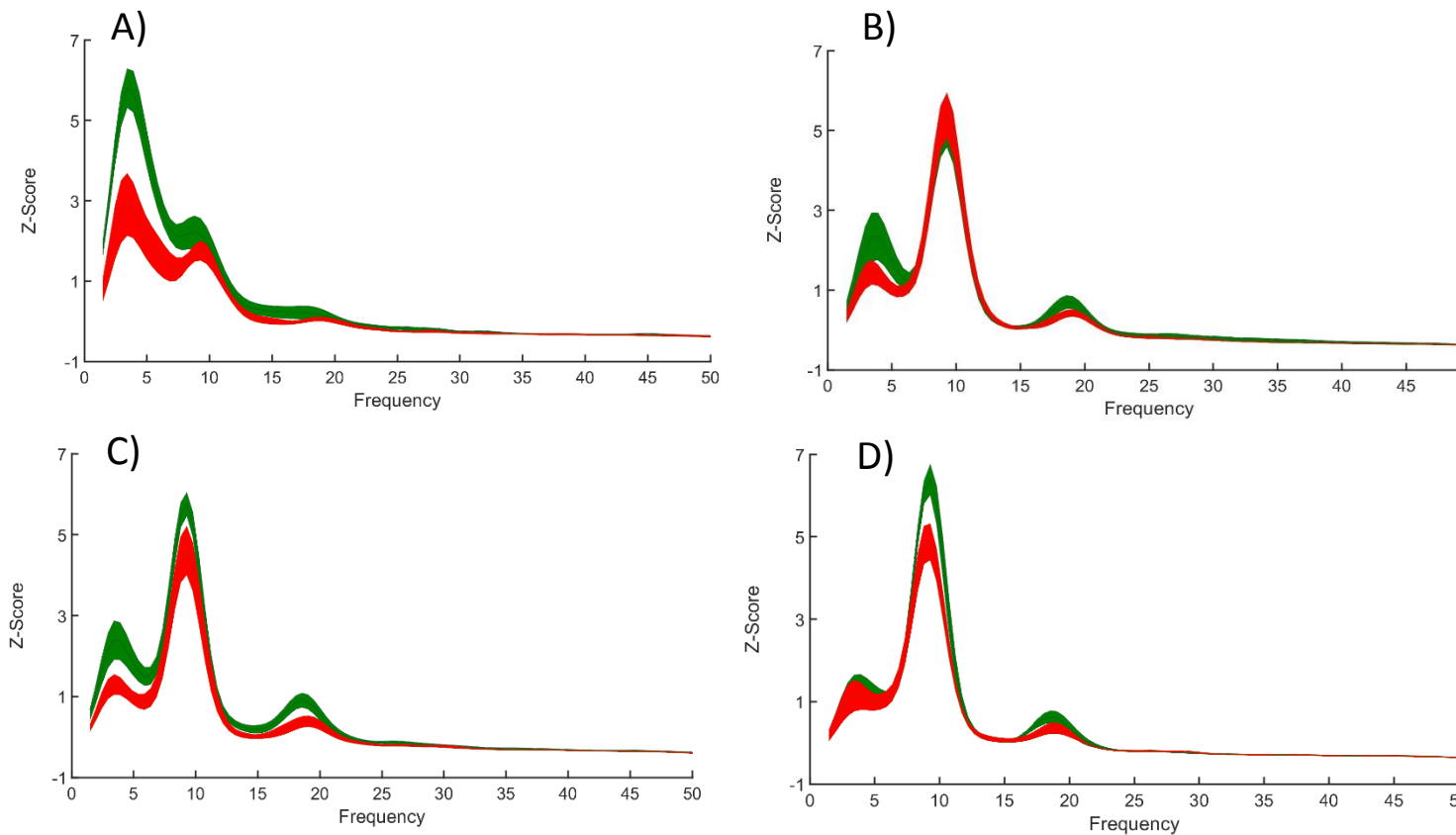*Figure 8: Mean normalized power ± SEM for sham rats entering novel (green) and repeat (red) arms as generated by the A) PFC, B) left HPC, C) right HPC, D) SUB. Peak power was lower for repeat arms in the higher theta frequency band, but other differences failed to reach significance (see text for details). Data were analysed separately for each of the following bands: Delta – 1-4Hz; Low theta – 4-8Hz; High theta 8-12Hz; Beta 13-29Hz; Low gamma 30-48Hz; High gamma – 52-100Hz*

Comparison of peak power between groups

When normalized peak power was compared directly between lesioned and sham rats (Figure 9), the right HPC showed a significant reduction in lesioned rats compared to shams in the high theta frequency band for entries to novel arms (Mann Whitney U = 3, Z = -2.208, *p* = .031, 99% confidence interval = .027 - .035). The right HPC also showed a further reduction for the delta frequency band for entries to repeat arms (Mann Whitney U = 3 Z = -2.208 *p* = .027 99% confidence interval = .027 - .035). The SUB was also a site of altered electrophysiology between groups, with lesioned rats generating significantly less power at high theta (Mann Whitney U = 3, Z = -2.208 *p* = .026 99% confidence interval = .023 - .03) when entering novel arms and significantly less power at high gamma (Mann Whitney U = 4, Z = -2.238 *p* = .049, 99% confidence interval = .044 - .055) upon entering repeat arms, evidenced in Figure 9.

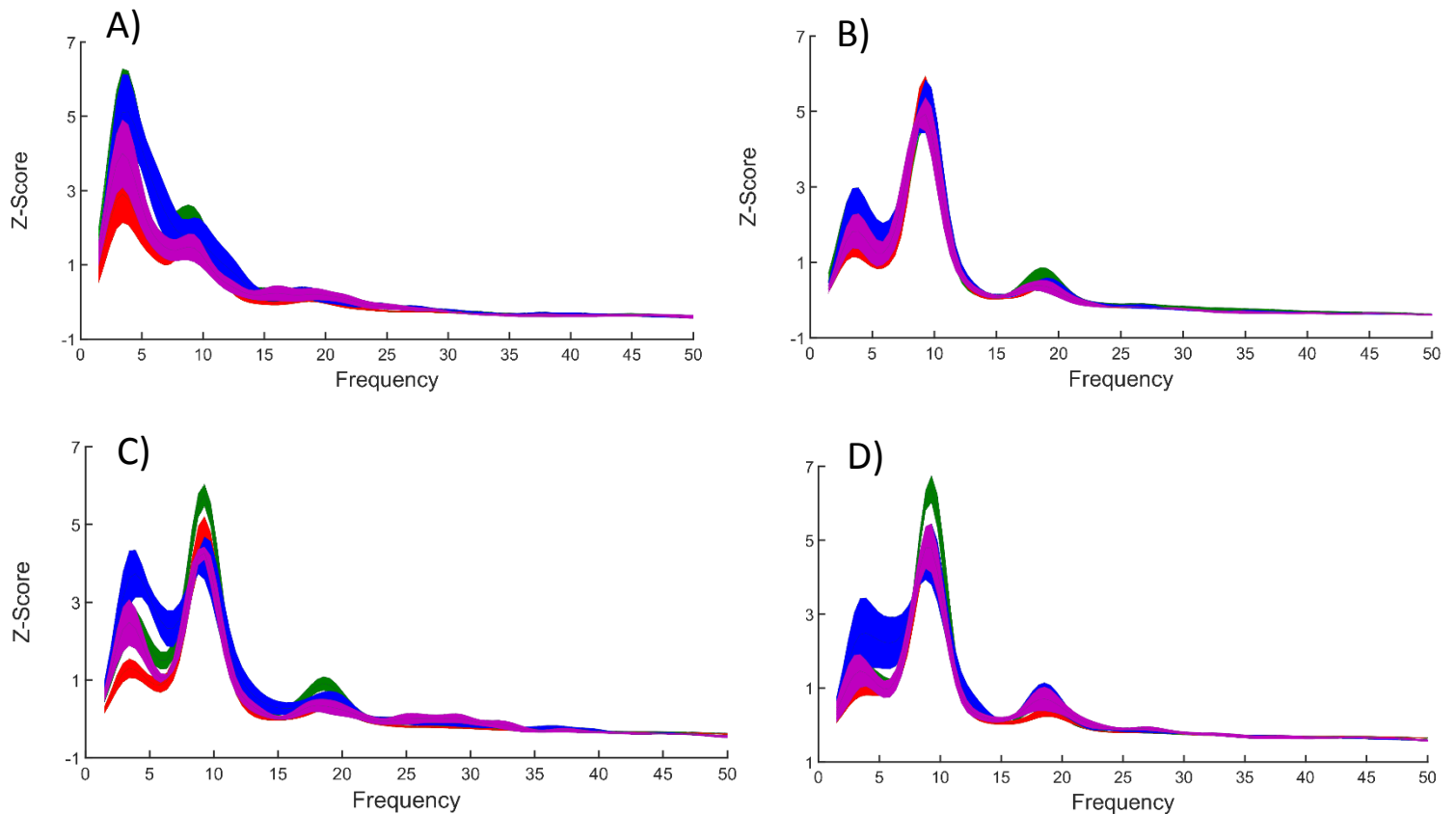# Normalized PSD for sham and lesioned rats entering novel and repeat arms

Figure 9: Mean normalized power ± SEM for sham and lesioned rats entering novel (sham = green; lesion = blue) and repeat (sham = red; lesion = purple) arms as generated by the A) PFC, B) left HPC, C) right HPC, D) SUB. There was a significant decrease in right HPC high theta in lesioned rats entering repeat arms, as well as a decrease in HPC delta, and SUB high theta and high gamma when entering repeat arms. Data were analysed separately for each of the following bands: Delta – 1-4Hz; Low theta – 4-8Hz; High theta 8-12Hz; Beta 13-29Hz; Low gamma 30-48Hz; High gamma – 52-100Hz

Coherence

Coherence within groups during novel and repeat arms

Analysis of coherence between the left HPC-PFC, left HPC- right HPC, and left HPC-SUB was analysed and compared within group for novel and repeat arms. There were no significant differences between novel and repeat choice coherence in the lesion group (Figure 10). Sham rats however showed reduced coherence between the HPC and all structures of interest at varying frequencies. In the sham group, there was a significant reduction in coherence when entering repeat arms vs novel between the HPC-PFC at high gamma frequency (Z = -2.197, p = .032, 99% confidence interval = .27 -. 36). There was also significantly less coherence at high gamma between the left HPC and right HPC (Z = -2.521 p = .01, 99% confidence interval = .008 - .013) when entering repeat vs novel arms. The HPC-SUB pair however showed the greatest changes in coherence between repeat vs novel arms, with reductions in coherence across beta, low gamma, and high gamma (All Z's > -2.2, all p < .05, 99% confidence interval = .024 - .032). Coherence values across structures in novel and repeat arms are shown in Figure 11.

Coherence in lesioned rats entering novel and repeat arms

Figure 10: Lesion group mean normalized ± SEM coherence values for novel (green) and repeat (red) arms across A) HPC-PFC B) HPC-HPC, and C) HPC-SUB. Width of lines equates to standard deviation of data. There were no significant differences in coherence between novel and repeat arms in any of these coherence measures. Data were analysed separately for each of the following bands: Delta – 1-4Hz; Low theta – 4-8Hz; High theta 8-12Hz; Beta 13-29Hz; Low gamma 30-48Hz; High gamma – 52-100Hz
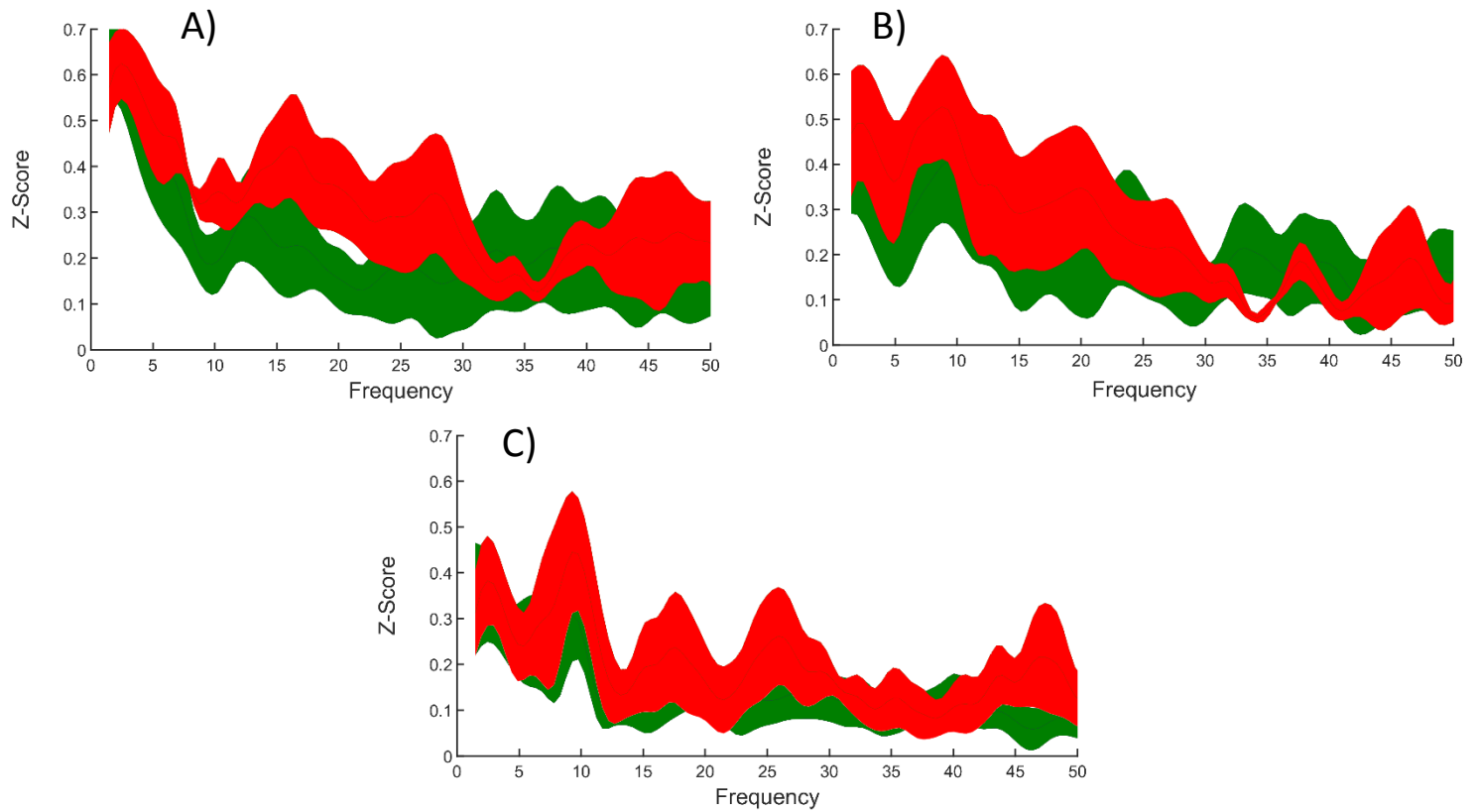
Coherence in sham rats entering novel and repeat arms
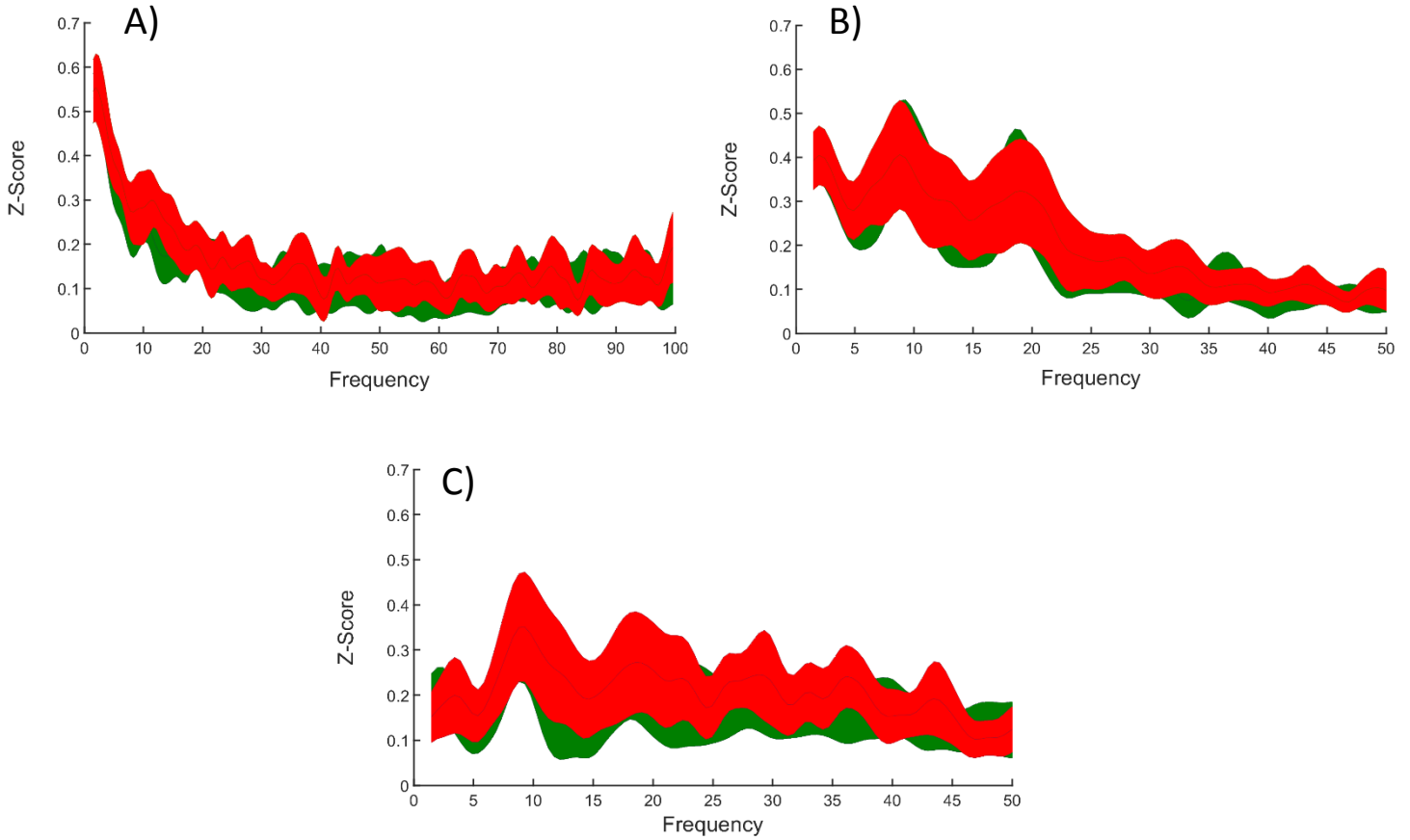
Figure 11: Sham group mean normalized coherence ± SEM values for novel (green) and repeat (red) arms across A) HPC-PFC B) HPC-HPC, and C) HPC-SUB. Width of lines equates to standard deviation of data. Coherence was significantly decreased at high gamma across all 3 of these coherence measures. Further reductions in beta and low gamma were also found between the HPC-SUB axis. Data were analysed separately for each of the following bands: Delta – 1-4Hz; Low theta – 4-8Hz; High theta 8-12Hz; Beta 13-29Hz; Low gamma 30-48Hz; High gamma – 52-100Hz

There were no significant differences between lesioned and sham animals either entering novel arms or repeat arms (Figure 12).

Coherence between lesioned and sham rats entering novel and repeat arms
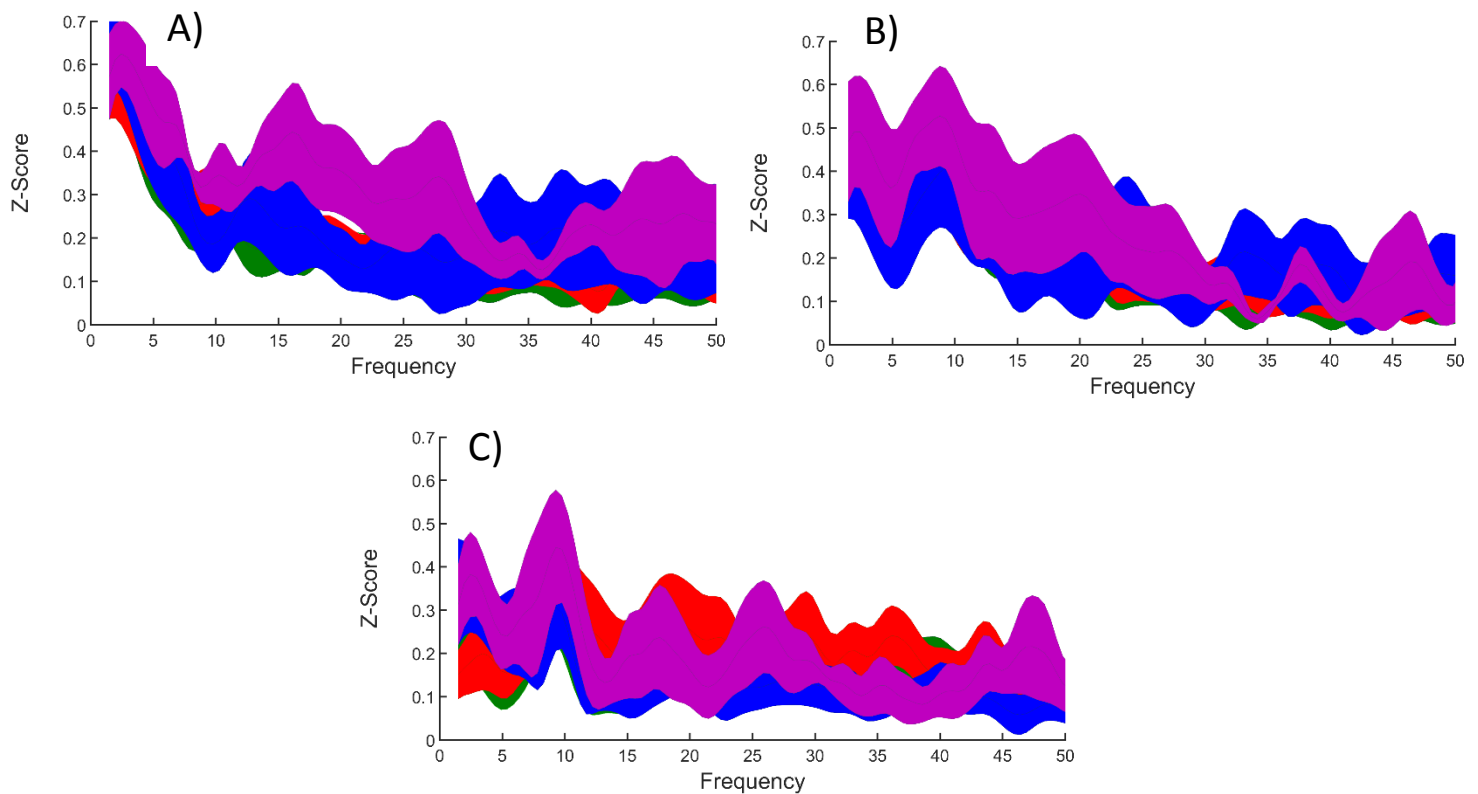
Figure 12: Mean normalized coherence ± SEM values between group for novel (sham = green, lesion =blue) and repeat (sham = red, lesion = purple) arms across A) HPC-PFC B) HPC-HPC, and C) HPC-SUB. Width of lines equates to standard deviation of data. There were no significant differences in coherence between novel and repeat arms in any of these axis. Data were analysed separately for each of the following bands: Delta – 1-4Hz; Low theta – 4-8Hz; High theta 8-12Hz; Beta 13-29Hz; Low gamma 30-48Hz; High gamma – 52-100Hz

Discussion:

45

The current study examined the effects of lesions to the ATN on the electrophysiology of other structures within the extended hippocampal memory system. The ATN is a crucial structure within this system due to its efferent and afferent connections to other memory structures, and damage to the ATN leads to memory impairment (Aggleton & Nelson, 2014; Kopelman, 2014; Dalrymple-Alford et al, 2015; Aggleton et al., 2016). The current study implanted microwire electrodes within the wider memory system, namely the PFC, bilaterally in the HPC, the RSP, and the SUB, to record rhythmic oscillatory activity from these structures while the rat was tested on a working memory task in the RAM. Previous studies have highlighted how damage to one component of the circuit can lead to changes at distal sites within the system (Jenkins et al, 2002; Aggleton, 2008; Vann and Albasser, 2009, Perry et al, 2018), but no previous study has used electrophysiological activity as a measure to examine impairment across the circuit. The main findings of the current study show altered electrophysiology both within sham rats entering repeat compared to novel, and between lesioned and sham rat groups. Sham rats appeared to show greater attenuation of electrophysiological activity when entering repeat arms compared to novel, with peak power reduced in a range of structures and frequencies in the intact sham animals. This difference was not found in rats with ATN lesions, which showed no significant within group difference between novel and repeat arms. Lesioned rats also showed reduced power for high theta (repeat and novel arms), delta, and high gamma (repeat arms only) compared to sham rats. This group difference may reflect poor performance in lesioned rats in the RAM task but further evidence is required for the 'forced choice' task.

The current study is the first to compare electrophysiological activity across structures in the extended hippocampal memory system after ATN lesions, giving a highly novel perspective as electrophysiology can examine 'real time' changes, whereas prior studies have used post-mortem histological measures to quantify lesion effects. All structures

of interest in the current study were chosen for their integral role in memory and thus may be expected to show altered electrophysiology during a memory task if the ATN was lesioned. The current study chose two electrophysiological measures to analyse, power and coherence. Power refers to the strength of signal at different frequency bands generated by each structure and was compared using peak power generated by each site. Coherence refers to the covariation of the amplitude of signals between two structures, or in other words, how much they are working together. In the current study the left HPC was the reference structure, so coherence values refer to the level of covariance in signal between our structures of interest and the left HPC.

Power Spectrum Density

There was a range of changes in electrophysiological power both within sham rats visiting novel verses repeat arms, and between lesioned and sham rat groups. Sham rats showed significant decreases in normalized PSD across multiple regions between novel and repeat arms. Specifically, low theta was decreased in the subiculum when entering repeat arms, as was delta and high theta in the PFC, and delta in the left HPC. This was not mirrored in lesioned rats, suggesting that lesions to the ATN may disrupt the attenuation of electrophysiological activity during behavioural testing.

The ATN may exert modulatory effects upon electrophysiology within the wider brain. Gibson et al. (2016) who used deep brain stimulation in pigs to show that stimulation of the ATN resulted in neural activation throughout the brain, including activation of the prefrontal, temporal, and sensorimotor cortex, and the hippocampus. This is further illustrated by Stykoplowski et al. (2014) using stimulation of under 40Hz in the sheep ATN to modulate hippocampal activity. These studies show that rather than simply being a node of communication for the extended hippocampal system, the ATN may play a vital role in

electrophysiological activity of other structures. Thus if the ATN is dysfunctional this electrophysiological regulation may not occur, which may explain why we found within group differences in sham but not lesioned rats**.**

Lesioned rats showed significantly less power than shams at delta in the right HPC, and less power at high theta and high gamma in the SUB when entering repeat arms. Lesions also reduced the power of high theta power in the right HPC when entering novel arms. As theta and gamma are both known to be involved in memory and recall processes, the current study supports literature that suggests that these electrophysiological signals may be reduced in the brain if memory is impaired. Gereke et al. (2018) used mice to illustrate that as familiarity with a behavioural paradigm increased, so too did theta, low gamma, and high gamma oscillations. This is supported by the current study as high theta and high gamma in the subiculum was decreased in lesioned animals when compared to shams when entering repeat arms verses novel arms. This may be because ATN lesions impaired the rat's development of familiarity within the RAM, and thus inhibited this increase in theta and gamma oscillation compared to the intact sham rats. Yamamoto et al. (2014) also showed that a surge in high gamma is observed before a 'correct' choice or before self-correcting a mistake in a behavioural paradigm in mice. This is consistent with the converse findings of the current study, that high gamma decreased in lesioned rats entering repeat arms compared to sham, as lesioned rats may not have been able to differentiate novel and repeat arm choices, thus abolishing the high gamma burst observed by Yamamoto et al (2014). There is also evidence suggesting that interactions between theta and gamma are critical to memory. Cross frequency coupling refers to the joining of different frequency band oscillations to facilitate memory function. Studies of cross frequency coupling show that gamma and theta oscillations may couple to form a mechanism that encodes and temporally orders memory (Jensen & Colgin, 2007; Nyhus & Curran, 2010). Although not tested in the current study this

may explain why both of these frequencies were weaker in lesioned rats compared to shams when entering repeat arms, as ATN damage and subsequent memory impairment may have altered the brains ability to produce this cross frequency coupling leading to reductions in power at both these frequencies in lesioned rats.

The current study showed a decrease in theta activity during the forced choice RAM paradigm. Theta is linked to encoding spatial memories, as well as allowing access to these memories at a later time (Fell & Axmacher, 2011; Colgin, 2011). Increases in theta activity in humans at time of encoding are often mirrored in recall, and can predict successful recall of information (Sederberg et al., 2003). If ATN damage inhibits the ability to properly encode memories, this burst in theta may be absent during their decision point in the current study, thus explaining why lesioned rats showed less power at high theta when presented with both novel and repeat arms.

There is evidence to suggest that oscillations in theta and gamma are integral to memory coding of environments and objects (Siegal et al, 2009) and that these frequencies may work to facilitate mnemonic processing, or to coordinate interactions between other neural structures during mnemonic processing (Tort et al., 2009; Sweeney-Reed et al., 2014; Heusser et al., 2016). Given the differences in lesioned rats during the repeat arm visits in the current study, the decrease in power of theta and gamma may be a reflection of a lack of impaired mnemonic processing in the novel arm stage, subsequently leading to unfamiliarity or lack of recall in the repeat arm tests.

Coherence

Coherence refers to the covariation in amplitude of frequency bands across sites. In the current study coherence was referenced to the left HPC, and analysed across the PFC, right HPC, and SUB. This gives the current study 3 pairs of structures with which to analyse

coherence; left HPC and PFC, left HPC and right HPC, and left HPC and SUB. The current study found significant differences in coherence between novel and repeat arms in sham rats. Coherence was decreased at high gamma across all pairs of structures examined in the current study (PFC-HPC, HPC-HPC, HPC-SUB) as well as additional decreases in synchrony being evident at beta and low gamma between the HPC-SUB. Significant differences between novel and repeat arms were restricted to sham rats, and no differences in coherence were found between lesion and sham groups. This suggests that an intact ATN regulates coherence in the wider memory system, decreasing synchrony across structures when the rat is faced with a 'familiar' (repeat) choice. While no changes in alpha, low theta, or high theta coherence were identified in either group, changes in high gamma were established across all pairs of structures (as well as decreased beta between HPC-SUB). Gamma oscillations are present in rats during exploratory behaviour (Chrobak & Buzsaki, 1998) which may in part explain the decrease in coherence at this frequency, as in rats with an intact ATN (thus unimpaired memory) gamma coherence may have been reduced when entering repeat arms as the rat was no longer 'exploring' a novel arm, whereas if the ATN is dysfunctional coherence at this frequency may have remained at the level of novel arm exploration, thus giving no significant differences in lesioned animals between novel and repeat arms.

The subiculum was a key site of reductions in coherence in the current study. While high gamma was decreased in sham rats during repeat arm visits across all pairs of structures, only the HPC-SUB axis showed any significant reduction at beta and low gamma frequencies. The subiculum is a major output of the HPC, and shares connections with the ATN that are not found in other HPC structures (Aggleton & Christiansen, 2015). This may explain why the HPC-SUB pairing was a crucial site for altered coherence, as if the ATN has a role in the generation or regulation of electrophysiological signals from other sites within the system, then a dysfunctional ATN may mean that the signal to regulate coherence is not

transmitted to the SUB, thus explaining why only sham rats showed significant reductions in coherence between HPC-SUB.

Limitations

A number of limitations should be considered for future work. First the sample size for the current project was smaller than was planned. Originally the study planned a sample size of 12 sham rats and 12 lesioned rats, but time constraints due to the nature of the project meant only 7 lesioned rats and 9 sham rats could undergo electrode implantation. Following this, 3 rats were excluded from the lesion group due to insufficient lesions and 1 was excluded from the sham group due to inaccurately placed electrodes, leaving a final sample of 4 lesioned and 8 sham rats. Future studies should account for the possibility of insufficient lesions and misplaced electrodes when establishing sample size.

A second issue in the current study was that the rats were ~ 2 years old at the time of testing and electrophysiological recording. This was due to the rats already being >1 year old when ethical consent was granted for the current study. PVG rats have a lifespan of around 2.5 years in our lab, so it may be that younger rats would have provided clearer examples of differences in electrophysiological activity. Future studies should begin with younger rats to avoid this issue.

There were also some issues with the electrophysiological recording equipment used in the current study. The measure used to establish latency (time of door lowering to time of 1st beam break) was dependent on a manual clicker to be pressed upon the door being lowered, but attaching this clicker to the random pulse generator was not as simple as expected. Signals were intermittently missed, reducing the validity of this latency measure to indicate accurate performance. However, because the electrophysiological epochs analysed in the current study were taken from -.2s to -.7s from the 1st beam break being broken, this did

not influence the validity of results. Future studies may wish to design an automatic measure of recording door lowering so as not to rely on the manual input of the researcher.

Future directions

The current study has paved the way for many future directions in this research. Other than Dr Brook Perry's work in MTT lesions, no other study has looked at changes in a dynamic measure such as electrophysiology within the context of lesions the extended hippocampal memory system. Future work could focus on lesions or electrode implantation in other structures within the system to further elucidate the complex interactions between the neural structures in this memory circuit.

Future work could also investigate cross frequency coupling across extended hippocampal memory circuit components. Of particular interest may be gamma and theta cross frequency coupling within and between structures within the extended hippocampal system as previous research has shown these frequencies to be critical in memory.

Conclusion

In summary, the current study provides novel insight into the electrophysiology of rats with lesions to the anterior thalamic nuclei. Sham rats, but not lesioned rats, demonstrated decreases in power at delta and high theta when entering novel arms compared to entering repeat arms, and in low theta upon entering novel arms. There was also a between group difference with lesioned rats showing significantly reduced power compared to shams at delta, high theta, and high gamma when entering repeat arms. Differences in coherence were only found within the sham group entering repeat arms verses novel arms. There were no differences in lesioned rat coherence within group, or any significant differences between sham and lesion groups as a whole. The overall findings of the study suggest that the ATN may play a modulatory role in the electrophysiological activity of the wider system. That is,

changes in electrophysiology may be a result of the ATN regulating neural activity through its manifold connections to other memory structures. If the ATN is damaged or dysfunctional, this regulation may not occur giving rise to the changes found in sham rats as opposed to lesioned rats in the current study. Such changes may be particularly relevant to the view that the ATN provides a nodal point in the extended hippocampal memory system (Aggleton & Brown, 1999, Dalrymple-Alford et al, 2015). These changes may also underpin memory problems in human clinical amnesia patients (Aggleton et al, 2016).

References

Aggleton, J., & Brown, M. (1999). Episodic memory, amnesia, and the hippocampal–anterior thalamic axis. *Behavioral and Brain Sciences*, 22(3), 425-444.

Aggleton, J. P., & Christiansen, K. (2015). The subiculum: the heart of the extended hippocampal system. *In Progress in brain research* (Vol. 219, pp. 65-82). Elsevier.

Aggleton, J. P., & Nelson, A. J. (2015). Why do lesions in the rodent anterior thalamic nuclei cause such severe spatial deficits?. *Neuroscience & Biobehavioral Reviews*, 54, 131-144.

Aggleton, J. P., Pralus, A., Nelson, A. J., & Hornberger, M. (2016). Thalamic pathology and memory loss in early Alzheimer's disease: moving the focus from the medial temporal lobe to Papez circuit. *Brain,* 139(7), 1877-1890

Buzsáki, G., Anastassiou, C. A., & Koch, C. 2012. The origin of extracellular fields and currents—EEG, ECoG, LFP and spikes. *Nature reviews neuroscience*, 13(6), 407-420.

Carlesimo, G.A., Lombardi, M.G., Caltagirone, C., (2011). Vascular thalamic amnesia: areappraisal. *Neuropsychologia* 49, 777–789.

Chrobak, J. J., & Buzsáki, G. (1998). Gamma oscillations in the entorhinal cortex of the freely behaving rat. *Journal of Neuroscience*, *18*(1), 388-398.

Clarke, S., Assal, G., Bogousslavsky, J., Regli, F., Townsend, D. W., Leenders, K. L., & Blecic, S. (1994). Pure amnesia after unilateral left polar thalamic infarct: topographic and sequential neuropsychological and metabolic (PET) correlations. *Journal of Neurology, Neurosurgery & Psychiatry*, 57(1), 27-34

Colgin, L. L. (2011). Oscillations and hippocampal–prefrontal synchrony. *Current opinion in neurobiology*, 21(3), 467-474.

Colgin, L. L. (2013). Mechanisms and functions of theta rhythms. *Annual review of neuroscience*, 36, 295-312.

Curtis, C. E., & D'Esposito, M. (2003). Persistent activity in the prefrontal cortex during working memory. *Trends in cognitive sciences*, 7(9), 415-423.

Dalrymple-Alford, J. C., Harland, B., Loukavenko, E. A., Perry, B., Mercer, S., Collings, D. A., . . . Wolff, M. (2015). Anterior thalamic nuclei lesions and recovery of function: Relevance to cognitive thalamus. *Neuroscience & Biobehavioral Reviews*.

Dillingham, C. M., Frizzati, A., Nelson, A. J., & Vann, S. D. (2015). How do mammillary body inputs contribute to anterior thalamic function*?. Neuroscience & Biobehavioral Reviews,* 54, 108-119.

Dumont, J. R., Petrides, M., & Sziklas, V. (2010). Fornix and retrosplenial contribution to a hippocampo-thalamic circuit underlying conditional learning. *Behavioural Brain Research,* 209(1), 13-20.

Dumont, J. R., Amin, E., Wright, N. F., Dillingham, C. M., & Aggleton, J. P. (2015). The impact of fornix lesions in rats on spatial learning tasks sensitive to anterior thalamic and hippocampal damage. *Behavioural brain research*, 278, 360-374. Frizzarti et al., 2016

Dupire, A., Kant, P., Mons, N., Marchand, A. R., Coutureau, E., Dalrymple-Alford, J., & Wolff, M. (2013). A role for anterior thalamic nuclei in affective cognition: interaction with environmental conditions. *Hippocampus,* 23(5), 392-404.

Fell, J., & Axmacher, N. (2011). The role of phase synchronization in memory processes. *Nature reviews neuroscience*, 12(2), 105-118.

Gereke, B. J., Mably, A. J., & Colgin, L. L. (2017). Experience-dependent trends in CA1 theta and slow gamma rhythms in freely behaving mice. *Journal of neurophysiology*, *119*(2), 476-489.

Gibson, W. S., Ross, E. K., Han, S. R., Van Gompel, J. J., Min, H. K., & Lee, K. H. (2016). Anterior thalamic deep brain stimulation: functional activation patterns in a large animal model. *Brain stimulation*, *9*(5), 770-773.

Harland, B. C., Collings, D. A., McNaughton, N., Abraham, W. C., & Dalrymple-Alford, J. C. (2014). Anterior thalamic lesions reduce spine density in both hippocampal CA1 and retrosplenial cortex, but enrichment rescues CA1 spines only. *Hippocampus*, 24(10), 1232-1247.

Heusser, A. C., Poeppel, D., Ezzyat, Y., & Davachi, L. (2016). Episodic sequence memory is supported by a theta–gamma phase code. *Nature neuroscience*, 19(10), 1374.

Jankowski, M.M., Ronnqvist, K.C., Tsanov, M., Vann, S.D., Wright, N.F., Erichsen, J.T.,

Jensen, O., & Colgin, L. L. (2007). Cross-frequency coupling between neuronal oscillations. *Trends in cognitive sciences*, *11*(7), 267-269.

Aggleton, J.P., O'Mara, S.M.,(2013). The anterior thalamus provides a subcorticalcircuit supporting memory and spatial navigation. *Front. Syst. Neurosci*. 7, 45,eCollection 2013.

Jenkins, T. A., Dias, R., Amin, E., Brown, M. W., & Aggleton, J. P. (2002). Fos imaging reveals that lesions of the anterior thalamic nuclei produce widespread limbic hypoactivity in rats. *The Journal of neuroscience, 22*(12), 5230-5238.

Jones, M., Errington, M., French, P., Fine, A., Bliss, T., Garel, S., . . . Davis, S. (2001). A requirement for the immediate early gene Zif268 in the expression of late LTP and long-term memories. *Nature neuroscience, 4*(3), 289-296.

Jones, M. W., & Wilson, M. A. (2005). Theta rhythms coordinate hippocampal–prefrontal interactions in a spatial memory task. *PLoS biol*, 3(12), e402.

Ketz, N. A., Jensen, O., & O'Reilly, R. C. (2015). Thalamic pathways underlying prefrontal cortex–medial temporal lobe oscillatory interactions. *Trends in neurosciences*, *38*(1), 3-12.

Kim, J., Delcasso, S., & Lee, I. (2011). Neural correlates of object-in-place learning in hippocampus and prefrontal cortex. Journal of Neuroscience, 31(47), 16991-17006.

Kopelman, M. D. (2014). What does a comparison of the alcoholic Korsakoff syndrome and thalamic infarction tell us about thalamic amnesia? *Neuroscience & Biobehavioral Reviews*. doi: 10.1016/j.neubiorev.2014.08.014

Loukavenko, E. A., Wolff, M., Poirier, G. L., & Dalrymple-Alford, J. C. (2016). Impaired spatial working memory after anterior thalamic lesions: recovery with cerebrolysin and enrichment. *Brain Structure and Function*, 221(4), 1955-1970.

Manns, J. R., Zilli, E. A., Ong, K. C., Hasselmo, M. E., & Eichenbaum, H. (2007). Hippocampal CA1 spiking during encoding and retrieval: relation to theta phase. *Neurobiology of learning and memory*, *87*(1), 9-20.

Maris, E., & Oostenveld, R. (2007). Nonparametric statistical testing of EEG-and MEG-data. *Journal of neuroscience methods*, *164*(1), 177-190.

Maris, E., Schoffelen, J. M., & Fries, P. (2007). Nonparametric statistical testing of coherence differences. *Journal of neuroscience methods*, *163*(1), 161-175.

McNaughton, N., Ruan, M., & Woodnorth, M. A. (2006). Restoring theta-like rhythmicity in rats restores initial learning in the Morris water maze. *Hippocampus*, 16(12), 1102-1110.

Nyhus, E., & Curran, T. (2010). Functional role of gamma and theta oscillations in episodic memory. *Neuroscience & Biobehavioral Reviews*, *34*(7), 1023-1035.

Papez, J. W. (1937). A proposed mechanism of emotion. *Archives of Neurology & Psychiatry*, 38(4), 725-743.

Penke, Z., Morice, E., Veyrac, A., Gros, A., Chagneau, C., LeBlanc, P., . . . Davis, S. (2014). Zif268/Egr1 gain of function facilitates hippocampal synaptic plasticity and long-term spatial recognition memory. *Phil. Trans. R. Soc. B, 369*(1633), 20130159.

Perry, B. A., Mercer, S. A., Barnett, S. C., Lee, J., & Dalrymple-Alford, J. C. (2018). Anterior thalamic nuclei lesions have a greater impact than mammillothalamic tract lesions on the extended hippocampal system. *Hippocampus*, 28(2), 121-135.

Poirier, G., & Aggleton, J. (2009). Post-surgical interval and lesion location within the limbic thalamus determine extent of retrosplenial cortex immediate-early gene hypoactivity. *Neuroscience, 160*(2), 452-469.

Sanders, J. I., & Kepecs, A. (2014). A low-cost programmable pulse generator for physiology and behavior. *Frontiers in neuroengineering*, 7.

Sederberg, P. B., Kahana, M. J., Howard, M. W., Donner, E. J., & Madsen, J. R. (2003). Theta and gamma oscillations during encoding predict subsequent recall. *Journal of Neuroscience*, *23*(34), 10809-10814.

Siegel, M., Warden, M. R., & Miller, E. K. (2009). Phase-dependent neuronal coding of objects in short-term memory. *Proceedings of the National Academy of Sciences*, *106*(50), 21341-21346.

Spellman, T., Rigotti, M., Ahmari, S. E., Fusi, S., Gogos, J. A., & Gordon, J. A. (2015). Hippocampal–prefrontal input supports spatial encoding in working memory. N*ature*, 522(7556), 309.

Stypulkowski, P. H., Giftakis, J. E., & Billstrom, T. M. (2011). Development of a large animal model for investigation

Sweeney-Reed, C. M., Zaehle, T., Voges, J., Schmitt, F. C., Buentjen, L., Kopitzki, K., ... & Richardson-Klavehn, A. (2014). Corticothalamic phase synchrony and cross-frequency coupling predict human memory formation. *Elife*, 3.

Tischmeyer, W., & Grimm, R. (1999). Activation of immediate early genes and memory formation. *Cellular and Molecular Life Sciences* CMLS, 55(4), 564-574.

Tort, A. B., Komorowski, R. W., Manns, J. R., Kopell, N. J., & Eichenbaum, H. (2009). Theta–gamma coupling increases during the learning of item–context associations. *Proceedings of the National Academy of Sciences*, 106(49), 20942-20947.

Vann, S. D., & Albasser, M. M. (2009). Hippocampal, retrosplenial, and prefrontal hypoactivity in a model of diencephalic amnesia: Evidence towards an interdependent subcortical-cortical memory network. *Hippocampus, 19*(11), 1090-1102.

Vann, S. D., & Nelson, A. J. (2015). The mammillary bodies and memory: more than a hippocampal relay. *Progress in brain research, 219*, 163-185.

Yamamoto, J., Suh, J., Takeuchi, D., & Tonegawa, S. (2014). Successful execution of working memory linked to synchronized high-frequency gamma oscillations. *Cell*, *157*(4), 845-857.